Ore Geology Reviews 105 (2019) 551–571

Contents lists available at ScienceDirect

Ore Geology Reviews

journal homepage: www.elsevier.com/locate/oregeorev

Geology and geochemistry of the Kadamzhai and Chauvai gold-antimony-mercury deposits: Implications for new province of Carlin-type gold deposits at the Southern Tien Shan (Kyrgyzstan)

P.A. Nevolko[a,c,*], O.M. Hnylko[b], V.P. Mokrushnikov[a], A.S. Gibsher[a], Yu.O. Redin[a], F.I. Zhimulev[a], A.E. Drovzhak[b], T.V. Svetlitskaya[a], P.A. Fomynikh[a], M.I. Karavashkin[b]

[a] VS Sobolev Institute of Geology and Mineralogy, Siberian Branch of the Russian Academy of Sciences, 3 Koptyug Ave., 630090 Novosibirsk, Russia
[b] Institute of Geology and Geochemistry of Combustible Minerals, National Academy of Sciences of Ukraine, Naukova 3a, 79060 Lviv, Ukraine
[c] Novosibirsk State University, 2 Pirogova Str., 630090 Novosibirsk, Russia

ARTICLE INFO

Keywords:
Kadamzhai
Chauvai
Carlin-type gold deposits
Geochemistry
Southern Tien Shan
Kyrgyzstan

ABSTRACT

The Tien Shan Belt extends for over 2500 km, from western Uzbekistan, through Tajikistan, Kyrgyzstan and southern Kazakhstan to western China, and represents a part of the Altaid Orogenic Collage. The Tien Shan is one of the largest gold provinces on Earth and hosts several world-class gold deposits. The Turkestan-Alay and Southern Fergana regions, located within the South Tien Shan, host an important Hg–Sb mineral province with proven reserve of over 5 Mt Sb and 0.8 Mt Hg. In Soviet times, during the intensive study and exploitation of the mercury-antimony deposits, increased gold content of these ores has been noted. But the focus on only the main ore components (Hg-Sb), as well as the absence of "working" exploration geological and genetic models of Carlin type deposits, did not allow to fully assess the gold potential of the ore belt. Meanwhile, gold exploration in the region during the past two decades has identified a few deposits, now recognized as Carlin type. The studied Chauvai and Kadamzhai Hg-Sb deposits belong to the central part of the South Fergana antimony-mercury belt and, together with other Hg-Sb deposits (Abshyr, Khaidarkan), form a large ore province. They are located in the northern arms of the Alay ridge extending along the southern flank of the Kauzan antiform. The South Fergana antimony-mercury belt is commonly associated with the North-Katran regional deep fault (located between the southern edge of the Fergana depression and the foot of the Alay and Turkestan ridges). The host rocks are represented by alternating grey inequigranular gradational-layered sandstones, gravel, associated with sandstones by gradual transitions, and dark-grey carbonaceous siltstones, enriched in organic matter. Gold mineralization is confined to the main contact of the Tolubai Formation and Alay limestone. The rocks of the Tolubai Formation and Alay limestones have undergone pervasive hydrothermal alteration near the "main contact". Based on the study of host rocks, three main types of gold-associated alteration have been recognized, such as jasperoides, decarbonatization, and sulfidization. Mineral composition of the Kadamzhai and Chauvai deposits is similar to gold deposits located in Nevada and Guizhou province. These deposits contain both Au and Sb-Hg. The main minerals in gold ore are pyrite, marcasite, arsenopyrite, orpiment, and realgar. The Sb-Hg ores are represented by cinnabar and stibnite. Deposits contain invisible gold (no observed native gold) associated with arsenic, antimony, mercury, and thallium, and have high gold-silver ratios. The distribution of gold is structurally controlled and is disseminated in the wall rocks. Structural settings for gold mineralization at the Kadamzhai and Chauvai deposits are transpressional regime. Based on geology, geochemical signatures and mineral composition of the Kadamzhai and Chauvai deposits that these deposits can be classified as Carlin type.

1. Introduction

The Tien Shan Belt extends for over 2500 km, from western Uzbekistan, through Tajikistan, Kyrgyzstan and southern Kazakhstan to western China, and represents part of the Altaid Orogenic Collage (Sengör et al., 1993; Sengör and Natalin, 1996; Yakubchuk, 2004) of

* Corresponding author at: VS Sobolev Institute of Geology and Mineralogy, Siberian Branch of the Russian Academy of Sciences, 3 Koptyug Ave., 630090 Novosibirsk, Russia.
E-mail address: nevolko@igm.nsc.ru (P.A. Nevolko).

https://doi.org/10.1016/j.oregeorev.2018.12.014
Received 5 March 2018; Received in revised form 4 December 2018; Accepted 17 December 2018
Available online 18 December 2018
0169-1368/

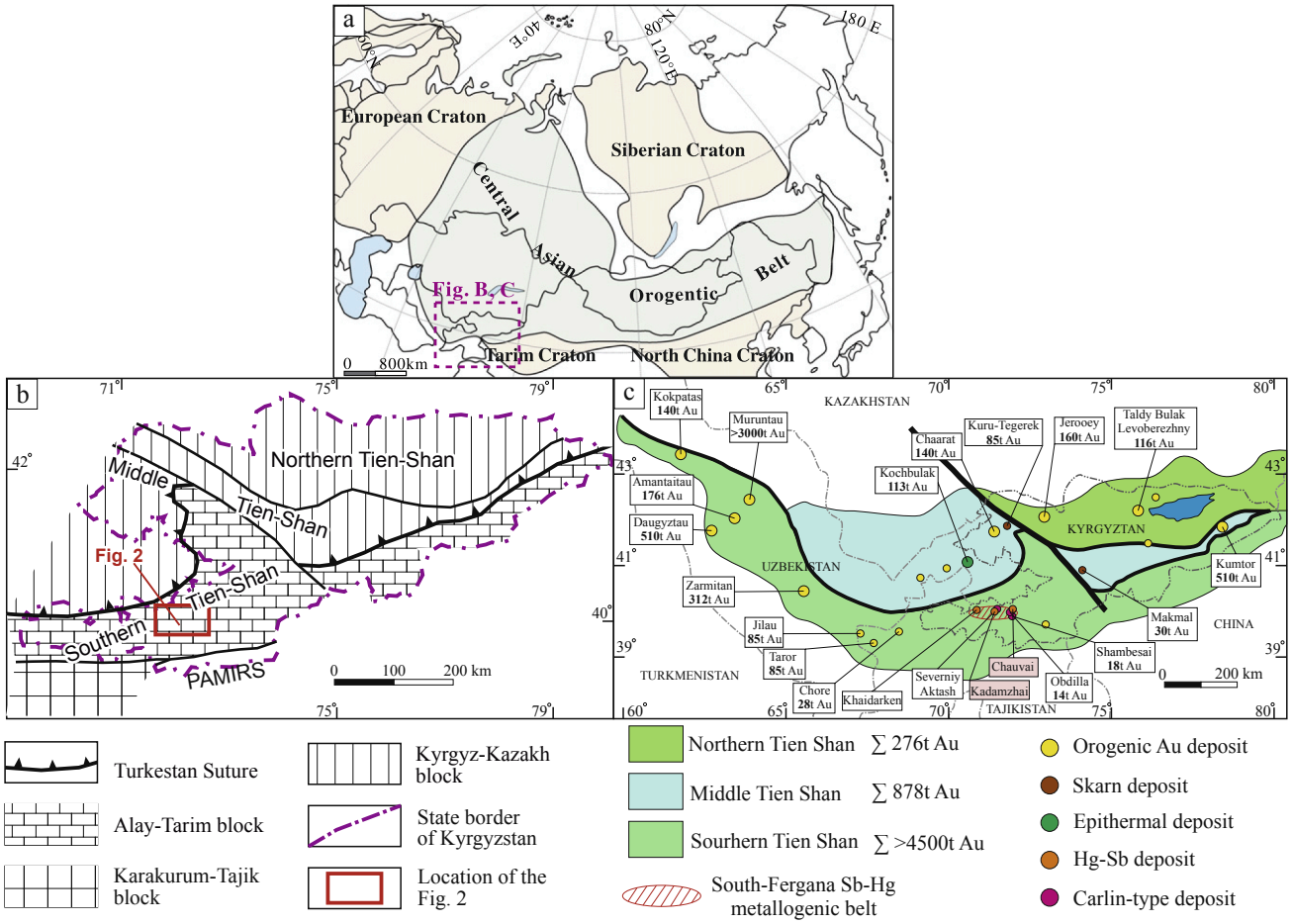

Fig. 1. (a) Tectonic outline of the Central Asia Orogenic Belt (modified from Jahn et al. (2000)). (b) The main tectonic units of Kyrgyztan (after Burtman (2006) and Biske and Seltmann (2010)). (c) Distribution of the most significant gold deposits in the Tien Shan Gold Belt (modified from Yakubchuk et al. (2002) and Goldfarb et al. (2014)).

central Eurasia (Fig. 1). The Tien Shan Gold Province coincides with a Paleozoic fold and thrust belt hosting numerous mesothermal gold deposits (Mao et al., 2004). It has undergone activation and orogenesis in the Alpine time and has become a part of the Himalayan orogenic belt formed by the Cenozoic collision of the Indian and Eurasian plates it is a hot spot for gold mining companies.

The Tien Shan is one of the largest gold provinces on Earth and hosts several world-class gold deposits (Fig. 1c) (Seltmann et al., 2003). Muruntau in Uzbekistan is the largest gold resource in Eurasia (originally containing 5400 tonnes (175 Moz) of gold at an open pit recovered grade of 3.4 g/t Au), and Kumtor in eastern Kyrgyzstan is one of the world's 10 largest gold mines (550 tonnes (17.5 Moz), of Au grading 2–6 g/t Au) (Yakubchuk et al., 2002; Mao et al., 2004; Porter, 2006).

The Turkestan-Alay and Southern Fergana regions in the South Tien Shan Orogen form an important Hg–Sb mineral province that contains a proven reserve of over 5 Mt Sb and 0.8 Mt Hg (Nikiforov, 1969; Li et al., 2010; Zhou et al., 2017). Within this domain mineralization is associated with the limestone at the contact with the overlying clastic sediments. These deposits occur within the highly folded and deformed units of the Alay Segment of the Southern Tien Shan, over 300 km of strike length. Two large Sb-Hg deposits are located at the studied area (Fig. 2) in the Southern Fergana region, which have been discovered in the early 20th century.

At Soviet times, during the intensive study and exploitation of mercury-antimony deposits of the Southern Fergana region, increased gold content of these ores has been obviously noted. But the focus on only the main ore components (Hg-Sb), as well as the absence of "working" exploration geological and genetic models of Carlin type deposits, did not allow to fully assess the gold-bearing potential of the ore belt. Meanwhile, gold exploration in the region during the past two decades has identified a few deposits, now recognized as Carlin type (Yakubchuk et al., 2002; Seltmann et al., 2004; Rickleman et al., 2011; Kirwin et al., 2017). Examples of such deposits are Severnyi Aktash, Obdilla and Shambesai (Rickleman et al., 2011; Goldfarb et al., 2014).

Sedimentary rock-hosted disseminated gold deposits have geologic features and geochemical signatures that are remarkably similar to those of sedimentary rock-hosted gold deposits in the United States and People's Republic of China. The size of deposits is as yet undetermined, but they each contain significant potential resources grading 1–5 g/t. Exploration and drilling are in progress at the deposits.

In this paper, we report new ore geology, geochemical signatures and mineral composition of the sedimentary gold deposits in the Southern Fergana region and discuss the deposit type in terms of a Carlin-type gold province.

2. Geological background

Well-exposed structures in the Tien Shan Paleozoic fold belt were formed during amalgamation of Eurasia (Biske and Seltmann (2010) and references therein). The Kyrgyz Tien Shan Mountains are traditionally subdivided into the Northern Tien Shan, Middle Tien Shan and Southern Tien Shan (Fig. 1).

In Kyrgyzstan, the Northern Tien Shan consists of several Precambrian metamorphic blocks and Cambrian to Lower Ordovician ophiolites with deeper marine sequences. These geological units are

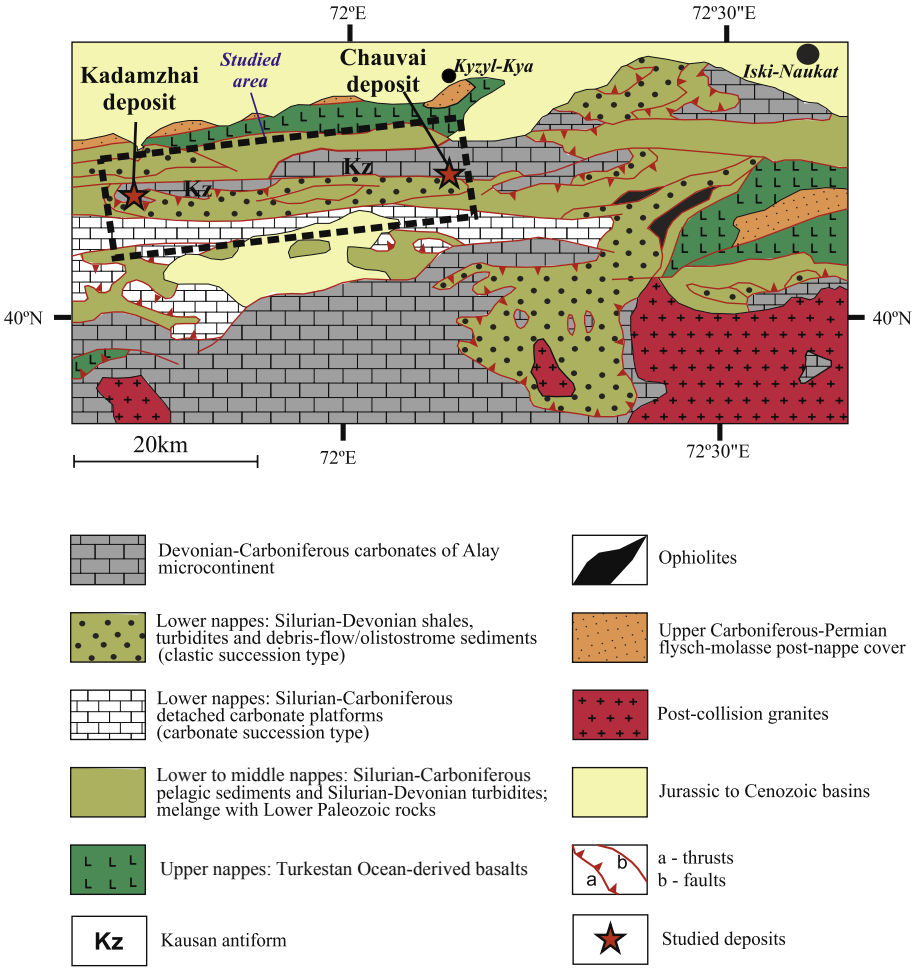

Fig. 2. The tectonic units of the northern branch of the Southern Tien Shan (Kadamzhai and Chauvai deposit area). According to Biske (personal communication, see also Biske (1996)).

overlain by Ordovician sediments and volcanic rocks and cut by I-type granites, ranging in age from Late Ordovician to Early Silurian. The main accretion occurred during the Ordovician (Ghes, 2008; Biske and Seltmann, 2010). The Middle Tien Shan terrane is a single block of continental crust with the Precambrian basement (Zubtsov et al., 1974; Windley, et al., 2007; Alekseev et al., 2009). It collided with the continental blocks of the Northern Tien Shan during the Ordovician. As a result, the new Kyrgyz-Kazakh continent had been formed (Burtman, 2006; Biske and Seltmann, 2010).

The Southern Tien Shan is a late Paleozoic fold-nappe belt which was formed in response to collision of the Kyrgyz-Kazakh continent with the Alay-Tarim and Karakurum-Tajik continental blocks (Fig. 1b). In Kyrgyzstan, the Southern Tien Shan includes reworked Paleozoic cover of the Alay-Tarim block (microcontinent) and the remnants of the adjacent (sub)oceanic crust. It is bounded from the north by the suture of the Turkestan Ocean that existed between the Kyrgyz-Kazakh and Alay-Tarim continents (Biske and Seltmann, 2010).

The studied (Figs. 1 and 2) area is situated in the mountain region to the south of the Fergana depression. It is a part of the northern (Bukantau–Kokshaal according to Biske (1996)) branch of the Southern Tien Shan. This branch was formed as a result of the Turkestan Ocean crust subducted beneath the active Kyrgyz-Kazakh continental margin and subsequently (after closure of the Turkestan Ocean in the Moscovian age) ubmerging northern passive margin of the Alay microcontinent (probably the western continuation of Tarim) into the subduction zone, which was inclined to the north. As a result, the fold-nappe belt was built with both ocean-derived slices and the detached Paleozoic predominantly sedimentary cover of the Alay microcontinent (Burtman, 2006; Biske and Seltmann, 2010 and references therein).

The upper nappes in the northern branch of the Southern Tien Shan are of oceanic (Turkestan Ocean) origin (Fig. 2) and are composed of Cambrian to Early Carboniferous ophiolitic fragments (ultramafic, gabbros, basalts and cherts) which are metamorphosed in blue-shale and eclogite facies (Burtman, 2006). Most basalts of the upper nappes erupted onto late Silurian to Devonian deep-sea sediments and thus are not related to the Ordovician ophiolites (Konopelko et al., 2018). Under them are the middle nappes filled by Silurian-Carboniferous predominantly pelagic deep-sea deposits (so-called condensed sedimentary succession represented by green, red, and black slates and cherts, laminated cherty limestones). The lower nappes are made up of Silurian to Devonian shales, turbidites and debris-flow/olistostrome deposits (clastic succession type) as well as the Silurian to Carboniferous carbonate platform sedimentary rocks (carbonate succession type). The (para)-autochthon consists of mainly Devonian to Carboniferous shallow-marine shelf-type dolomites and limestones of the Alay microcontinent (Alay succession type or simply Alay limestone).

Synorogenic Late Carboniferous turbidites were deposited on the top of many nappes and show the same rejuvenation of lower nappes in comparison with upper ones. Flysch is tectonically covered by overlying nappes. Such flysch is developed on top of Alay-type succession. It conformably lies on Alay limestone and is tectonically covered by the lower nappes comprising the Silurian to Devonian sediments (clastic succession type). The synorogenic flysch belongs to the Tolubai Formation (Moscovian in age) and is represented by gravel-sandy-clay-

marl turbidites including coarse submarine debris-flow deposits with large olistolites/olistoplaques, mainly comprised of limestones, in the upper part of the formation. Generally, the turbidites demonstrate coarsening of grains upwards the sedimentary sequence. These turbidites reach 1 km in thickness.

Tectonic melanges with fragments of lower to middle Paleozoic rocks are recorded in the South Fergana mountain region (Biske, 1996; Biske and Seltmann, 2010 and citation therein). In some places, post-nappe cover is developed and represented by Carboniferous to Permian flysch and molasse sediments.

The package of tectonic nappes was deformed into folds (antiforms and synforms) as a result of further collisional compression in the late Paleozoic. The Kausan antiform (see Fig. 2) is one of such structures hosting the Sb-Hg deposits of Kadamzhai and Chauvai. Additionally at this time, the South Tien Shan orogen fragment by predominantly subvertical strike-slip faults.

Post-collisional granitoid intrusions of the Alay segment are generally undeformed and demonstrate crosscutting relationships with all late Paleozoic sedimentary formations. The intrusions are exposed in the axial parts of the Alai range (Fig. 2), with detailed descriptions of main rock-types and characterization of post-collisional magmatism (Osmonbetov and Knauf, 1982; Dodonova et al., 1984; Nenakhov et al., 1992; Nenakhov and Vaulin, 1992; Nenakhov and Belov, 1996; Solomovich, 2007). According to Konopelko et al. (2018), diverse magmatic series of the Alai segment formed virtually coevally in a post-collisional setting during the main post-collisional magmatic pulse at 290–280 Ma, which is similar to ages of post-collisional intrusions elsewhere in the Southern Tien Shan.

In Mesozoic-Cenozoic time, this territory developed a platform regime. In the Alpine stage, a modern high-mountain topography was formed, as well as new faults and gentle folds were originated due to collision of India and Eurasia.

3. Deposit geology

The Chauvai and Kadamzhai Hg-Sb deposits belong to the central part of the South Fergana antimony-mercury belt, which together with other Hg-Sb deposits (Abshyr, Khaidarkan) form a large ore province. They are located in the northern arms of the Alay Ridge extending along the southern flank of the Kauzan antiform (Fig. 2). The South Fergana antimony-mercury belt is commonly associated with the zone of the North-Katran regional deep fault (located between the southern edge of the Fergana depression and the foot of the Alay and Turkestan ridges).

3.1. Chauvai deposit

At the Chauvai ore field, the Carboniferous Alay limestones and overlapping synorogenic flysch of the Tolubai Formation, which is complicated by NE striking disjunctive dislocations and the low-order folding and is accompanied by sulfide mineralization, are developed (Nikiforov, 1969; Vaulyn, 2016). The ore field includes a few deposits and occurrences (Tuyuksai, Zor-Dange, Tolubai-Kyshtau, Tokunsai, Sart-Istagan, Dzhidasai, Kosh-Unkur, Chiltan, Chatmazar, Duvana-Tash) localized at the transition from the Alay limestone and the Upper Carboniferous synorogenic flysch of the Tolubai Formation (Fig. 3).

In the top portion of the Alay limestone succession, one can observe hydrothermal alterations expressed by jasperoides (silicification), which includes a Hg-Sb mineralization occurring as veinlets of antimonite and cinnabar. The thickness of jasperoids varies from 30 cm to 10 m. The Tolubai Formation contains interbedded sandstones, gravel, carbonaceous slates of siltstones and mudstones and rare occurrence of limestone lenses. At the base of the formation, the sedimentary rocks are reworked and transformed into the silicified tectonic breccia. The thickness of sandstones typically increases (up to 1 m) in the lower part of the formation, where they alternate with black carbonaceous slates of siltstones and mudstones. The middle part of the Tolubai Formation contains the intraformational clay limestones (up to 2–3 m thick), while the coarse-grained deposits (sandstones with gradual transition to gravels) prevail over the fine-grained varieties (carbonaceous, gray to dark gray siltstones and mudstones). The upper part is represented mainly by dark gray siltstones and argillites with thin interlayers of gray sandstones (up to 20 cm thick). Blocks of the massive gray limestones and dolomites tectonically occur above the Tolubai Formation (Fig. 4).

The sediments of the Tolubai Formation were crosscut by numerous strike-slip dislocations which are responsible for presence of irregularly-striking breccia layers composed of fragments of sandstones and siltstone with carbonate matrix and multidirectional calcite veinlets. The wide occurrence of silicified breccias in the basement of the Tolubai Formation as well as intensive brecciation and foliation of jasperoids and limestones of the Alay succession type suggest tectonic contact between these two units (however, there are local sites with concordant occurrence).

Gold mineralization at the Chauvai deposit is localized mainly in the near-contact zone (so called “main contact”, here and elsewhere this term means the contact between the Tolubai Formation and the Alay limestone) in the lower part of the Tolubai Formation. Economic mineralization is confined to clastic rocks, whereas gold content in jasperoid bodies rarely reaches 0.5 ppm. The main ore-controlling structure within the Chauvai deposit is a regional dislocation with strike-thrust kinematics. Significant gold contents have also been recorded in other parts of the Tolubai Formation and are most commonly associated with disjunctive dislocations of the strike-thrust kinematics of the lower order.

3.2. Kadamzhai deposit

A detailed mapping was carried out on the western flank of the Kadamzhai field, including the Karabiy and Slantsevyi Klin sites. Here, two main tectonic units of the northern (Bukantau-Kokshal after Biske (1996)) branch of the southern Tien Shan fold belt are developed. The first unit (parautochthone) is represented by the Carboniferous Alay limestone and the overlapping synorogenic flysch of the Tolubai Formation. Debris-flow/olistostrome sediments are also developed in the upper part of the synorogenic formation.

The second unit (allochthon: lower and middle nappes of the southern Tien) is made up of the Silurian to Devonian shales, turbidites (clastic succession type) and, locally, pelagic siliceous sediments (condensed sedimentary succession type). The Silurian to Devonian schists are locally transformed into clay mélange, including blocks of older early Paleozoic or Ediacaran (?) phtanites.

Parautochthone together with overlying lower and middle nappes is deformed into the antiform and synform folds. The core part of such an antiform (Kausan antiform) is composed of the Alay limestone and is exposed at the northern margin of the studied area (Aktash mountain; Figs. 2 and 5), while the flank of this antiform, filled predominantly with the Silurian to Devonian clastic sediments, is developed in the southern part of the area.

The Kausan antiform in the western part is severely disturbed by the younger shear-type faults, resulting in formation of the so-called “Slantsevyi Klin” (the so-named site; Fig. 5). In places, the “Slantsevyi Klin” site is characterized by a poor occurrence or even absence of the synorogenic flysch of the Tolubai Formation, resulting probably from the “tectonic peeling” of the flysch sedimentary succession during the sheet thrusting.

In the eastern part of the mapped area (the Karabiy mountains), the Alay limestones are delaminated into tectonic sheets, exfoliating from the main limestone body, thinning southward and wedging into flysch sediments of the Tolubai Formation (Fig. 5). To the south, these tectonic limestone wedges are occasionally replaced by olistostromic lenses in the Tolubai formation, suggesting consedimental protruding of limestone wedges into the flysch basin.

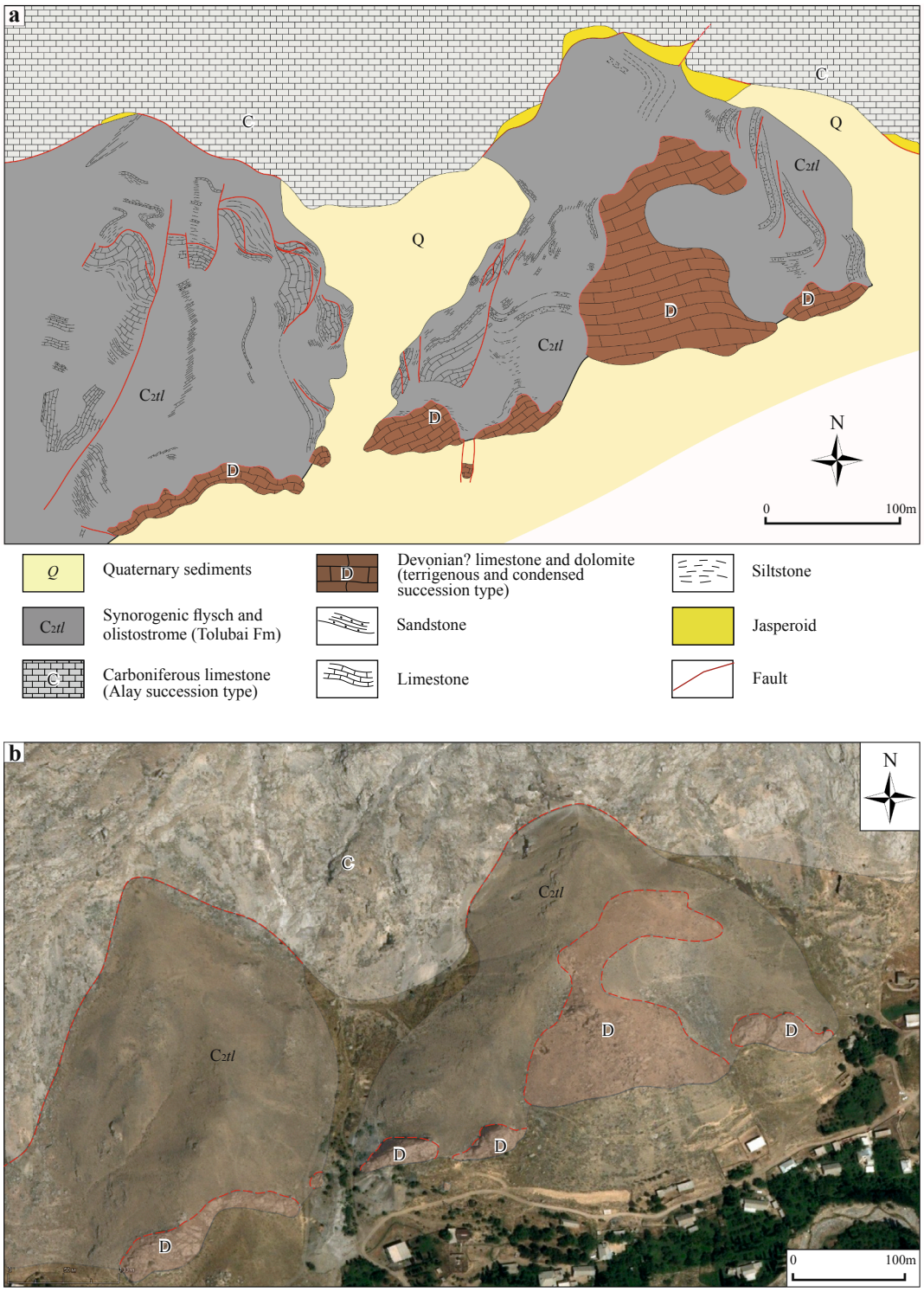

Fig. 3. (a) Detailed geological map of central part of the Chauvai deposit; (b) Simplified geological map of central part of the Chauvai deposit (satellite image from www.bing.com).

Silicification is distinctly manifested along the "main contact" of the clastic rocks of the Tolubai Formation and Alay- limestones. Both limestones and clastic rocks are fully or partially silicified. Tectonic breccias and debris-flow deposits are typical for the silicified rocks. Silicified rocks are commonly intensely ferruginized. Lack of the Tolubai Formation causes occurring the silicified limestones immediately under of the nappe of the Silurian to Devonian sediments (clastic succession type).

It should be noted that the sizes of silicification bodies (including jasperoids) increase from the east to the west, reaching first hundreds of meters in size in the "Slantsevyi Klin" site (Fig. 5). The gold content in these breccias reaches as much as 1–3 ppm.

3.3. Obdilla and Shambesai deposits

Geology of the Obdilla and Shambesai area is dominated by two east-west trends that are duplicates of the same succession, created by imbricate thrusting. Notably, the two deposits occur along the same

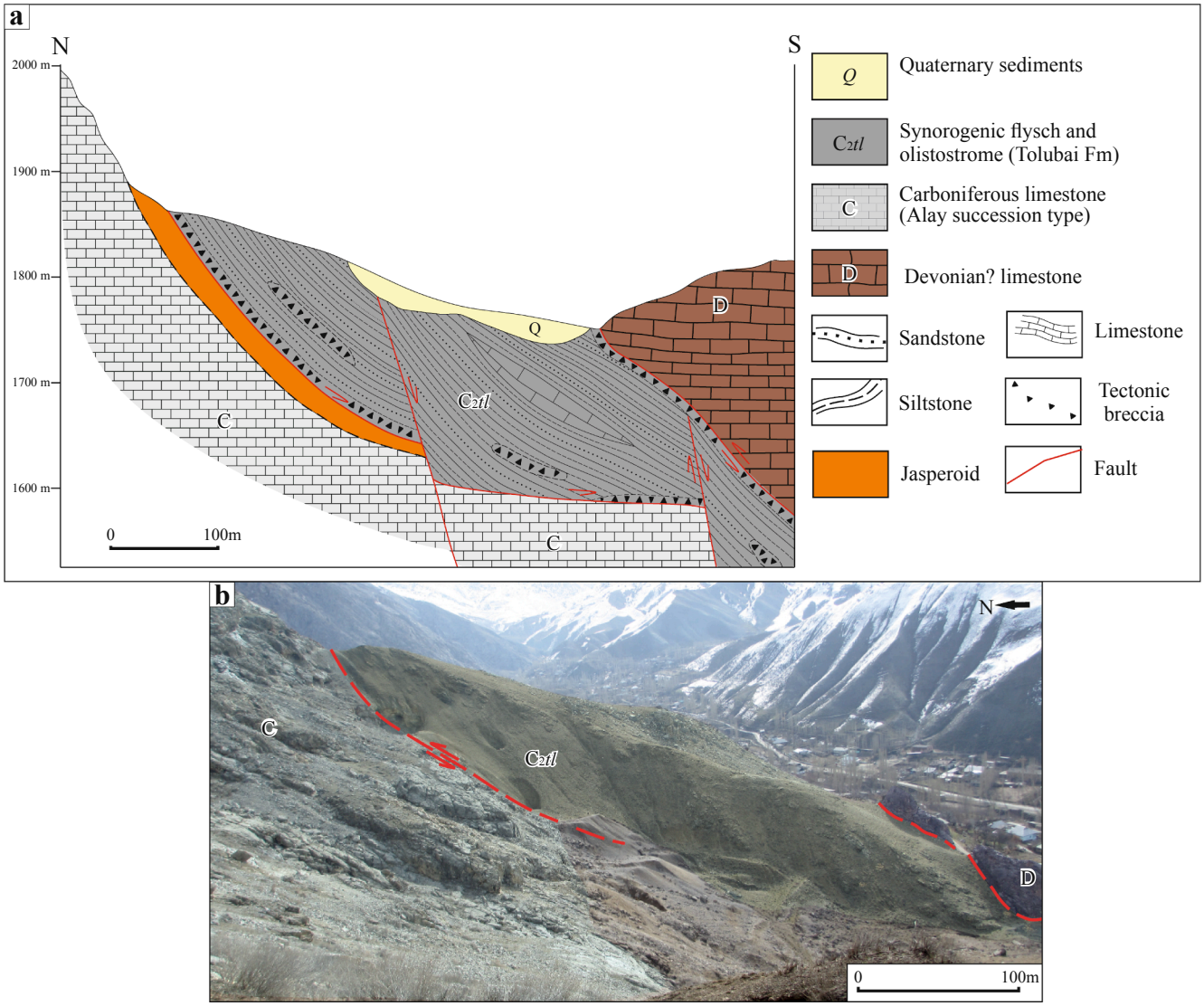

Fig. 4. (a) Conceptual cross section of the Chauvai deposit (modify after Kirwin et al. (2017)); (b) Photograph showing the contact between main geological units at the Chauvai deposit.

stratigraphic contact within each trend. Silurian siltstones, sandstones, shales and Devonian siltstone, cherty siltstones, limestone, and dolomite have been thrust onto Carboniferous limestone and carbonaceous siltstone. It is the south dipping contact between these Carboniferous units – the Pyrkaf Formation (massive reef Alay limestone) and the Tolubai Formation (carbonaceous, carbonate siltstone and fore-reef collapse breccias), which host both the Shambesai and Obdilla deposits. There are no intrusives, in the area.

The Shambesai orebody strikes ENE for 1.4 km, with 300 m wide and 30 m thickness. Gold mineralization occurs primarily in a sub-horizontal 'trough', on the contact formed by pre or synmineralization deformation. The tectonic breccia within this interval is the primary host of gold mineralization. Un-brecciated siltstone does carry grade, but only when proximal to a brecciated zone. Organic carbon is common in the upper siltstone. Limestone blocks, interpreted as likely debris from the reef-front, occur within the siltstone and also host mineralization at their boundary. Massive limestone is barren except where strongly brecciated < 1 m from the contact. Notably, the oxidation profile is inverted so that sulfide ore occurs above oxide ore, which is invariably found at the limestone contact. Oxide ore has been found in the deepest drilling at a depth of 409 m. This is probably due to meteoric water flowing along the contact (Rickleman et al., 2011). Gold is disseminated. Its size is 50 μm in oxide ore. Oxide ore has goethite often as sulfide pseudomorphs. Sulfide is generally extremely fine pyrite and arsenopyrite, although arsenopyrite is up to 20 μm in size. Realgar and orpiment occur with sulfide ore. Mineralized rock is decarbonatized, giving a 'pock-marked' texture and minor vugginess. Quartz veins, silicification and jasperoids occur but are not pervasive. Argillic alteration exists throughout the deposit however a clear zonation is not apparent (Rickleman et al., 2011).

The Obdilla ore body strikes east-west for 1.64 km, and is at most 220 m wide. The ore occurs as a sub vertical body that, while not related to the limestone contact as closely as Shambesai, does occur at a dip parallel to the Alay limestone. The controls on mineralization at Obdilla are far less well understood than at Shambesai, partly owing to the more complex shape of the ore body. Gold is disseminated and is at most 30 μm in size. Pyrite and arsenopyrite are the gold-bearing sulfides. Limonite and hematite occur throughout in minor amounts. Realgar, orpiment and cinnabar are also seen and chalcopyrite and magnetite in thin section only (Rickleman et al., 2011).

4. Sampling and analytical method

Local geology of the Kadamzhai and Chauvai deposits was studied

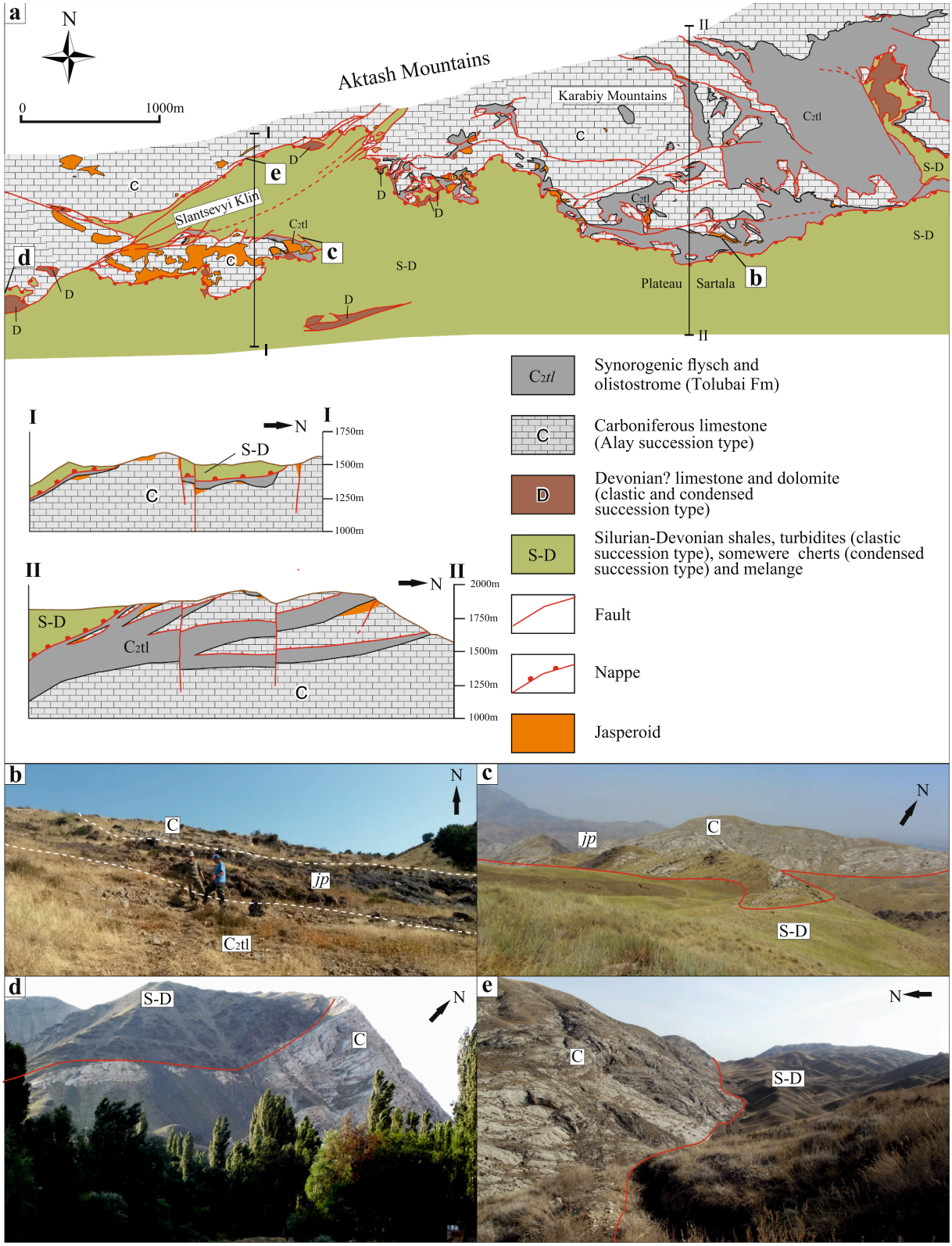

Fig. 5. (a) Geological map and cross-section of the eastern part of the Kadamzhai deposit. (b–e) Photographs showing the Kadamzhai deposit: (b) "Main contact" at the Karabiy Mountains; (c, e) "Main contact" at the Slantsevyi Klin; (d) A nappe structure at the left bank of the Shakhimardan River with Silurian-Devonian shales the Carboniferous Alay limestone.

during the large-scale geological mapping in 2017. We compiled detailed geological maps with a structural analysis of the localization of mineralization and hydrothermal alteration. At the Kadamzhai deposit, more than 100 samples were collected from surface, as well as from trenches. Most of the collected samples are oxidized, excluding strongly silicified breccias near the "main contact". Samples at the Chauvai deposit were collected from the surface, as well as from drillholes. The drillholes at the Chauvai deposit have been designed to cross the main

contact between the clastic rocks of the Tolubai Formation and the limestones of the Alay succession. In total, more than 500 samples were collected from 25 drillholes at the Chauvai deposit.

The mineral composition, textural–structural features, and mineral relations were studied under an optical microscope in reflected and transmitted light. A total of 120 polished sections and 10 thin sections from the Chauvai deposit and 30 polished and 10 thin sections from the Kadamzhai deposit, were studied to characterize the mineralogy, paragenetic and textural relationships, as well as petrography alteration types of host rocks.

The concentration of gold was analyzed by FAA (fire assay analysis with AA finish). Samples were fused with a mixture of lead oxide, sodium carbonate, borax, silica and other reagents as required, inquarted with 6 mg of gold-free silver and then cupelled to yield a precious metal bead. The bead was digested in 0.5 ml dilute nitric acid in the microwave oven, 0.5 ml concentrated hydrochloric acid was then added and the bead was further digested in the microwave at a lower power setting. The digested solution was cooled, diluted to a total volume of 10 ml with de-mineralized water, and then analyzed by atomic absorption spectroscopy against matrix-matched standards. Major and trace elements were analyzed by ICP-OES and ICP-MS reading (aqua regia digestion). Chemical analyses were performed in the Stewart Assay and Environmental Laboratories LLC, Kyrgyzstan. Detection limit is 0.01 ppm for Au, Bi, Nb, Ta, and U, 0.04 ppm for Rb, 0.1 ppm for Ba, Co, Sb, and Tl, 0.2 ppm for Mo and Sn, 0.4 ppm for Pb, 0.5 ppm for Cr, 1 ppm for Ag, Cu, Hg, Ni, V, and W, 1.5 ppm for As and Se, 2 ppm for Zn, 5 ppm for Sr and Te.

5. Results

5.1. Host rock lithology

The lithological characteristics of the host rocks of the Tolubai Formation within the Kadamzhai and Chauvai deposits are identical. The nature and scales of the hydrothermal alteration are also comparable. Hereafter, we provide a description of the host rocks according to the drilling data at the Chauvai deposit. Taking into account the lithological composition of the Tolubai sediments at the surface within the studied deposits, we suppose that the clastic rocks at the Kadamzhai and Chauvai deposits are similar.

The host rocks are represented by alternating grey heterogranular gradationally-layered sandstones, gravel associated with sandstones via gradational transitions, and dark-grey carbonaceous siltstones enriched in organic matter. Two elements are distinguished: (i) sandstone and gravel strata, varying in thickness from 5 to 120 cm; and (ii) packages of siltstones with thin sandstone layers. The quantitative proportions of coarse- and fine-grained rocks vary against the background of dominating sandstone.

The coarse-grained layers are characterized by gradational sorting of detrital material (Fig. 6a). The material grade directly correlates with the thickness of the layer. Gravel form the lower parts of the thickest layers of sandstones is 0.5–1.2 m thick. The clastic material of the sandstones is poorly rounded and sorted. The sandstones are wackes with a matrix of silt-clay material, part of some pores are filled with epigenetic carbonate material.

The base of coarse-grained layers is clear and even (Fig. 6b). The sandstones are represented by fine-grained varieties near the top of the strata, which are characterized by small cross wave-like lamination with finest interbeds of dark gray siltstones. Fine-grained sandstones and siltstones zone are thin (5–30 mm) alternating siltstone layers and fine-grained sandstone layers, 1–30 mm thick (Fig. 6c).

The breccia occurs at the base of the thickest layers of gravel with sandstone, the fragments of limestone “floating” in the gravel with sandstone matrix are common (Fig. 6d). The thickness of the breccia typically varies from 20 to 60 cm. The upper part of the Tolubai clastic succession contains blocks (olistoliths) of limestones and sequences of debris-flow sediments.

The clastic sediments of the Tolubai Formation outside the deposits occur conformably on Alay limestones. In some cases, there is a gradual transition from massive through platy limestones to clastic-carbonate rocks of the Tolubai Formation. Within the deposits, the contact is faulted, whereas the host rocks are hydrothermally altered. Mineralization is confined to the hydrothermally-altered rocks. The volume of altered host rocks varies greatly due to post-ore tectonic processes that disrupted the hydrothermal zonning. In some drill holes, the thickness of altered rocks may be as much as 20–40 m, while in other drill holes there is a tectonic contact between clasticrocks of the Tolubai Formation and unaltered limestones (wedging out of metasomatic alteration zone).

5.2. Specific features of the “main contact”

In the immediate vicinity of the main contact between the Tolubai Formation and Alay limestones, several zones can be recognized within the Tolubai Formation, whose appearance is determined both by the original sedimentation setting and superimposed alteration. The first zone is represented by a package of interbedding laminae of sandstones and siltstones (Fig. 6e). The sandstone laminae contain abundant disseminated sulfides (Fig. 6f). The specific feature of this zone is realgar and orpiment streaks whose wide occurrence corresponds to its lower part.

Towards the main contact, the rocks lose their bedded structure and acquire massive appearance due to deformations and subsequent hydrothermal alteration. This zone is conditionally called “massive siltstones”. In case of intense breccia structure, this zone may disappear from the sequence. Massive siltstones are not calcareous rocks including quartz and fluorite streaks, whereas sulfides occur as lenticular segregations and scattered dissemination (Fig. 6g). Massive siltstones are characterized by slight bleaching as compared to unaltered siltstones.

In the zone of massive siltstones, there is a gradual development of the breccia structure down the sequence with gradual transition to the breccia of the main contact. Breccia consists of angular debris of siltstones and sandstones. In some cases, the irregular bleaching is observed in spotted textures (Fig. 6h). Breccias are not calcareous, locally revealing silicified fine-grained cement, while rock fragments are silicified. Breccias are vesicular with caverns typically containing druses of fine-grained crystalline quartz. Breccia of the main contact differ from tectonic breccia of the Tolubai Formation. It has dense structure, high degree of lithification and bleaching, as well as elevated content and association of vein minerals and, locally, silicification.

Unaltered rocks of the Tolubai Formation are strongly calcareous. The massive siltstones and breccias of the main contact are typically not calcareous, while their thin interbedding packages can be represented by both calcareous and non-calcareous rocks. In some drillholes, the proportion of calcareous material gradually decreases down the sequence, but more frequently it disappears in the lower part of the thin interbedding zone.

The contact pattern with the Alay limestones can vary. If jasperoids (see below) are absent and breccias are in immediate contact with limestones, then the contact is distinct, but if jasperoids are present, then the contact can both be distinct (Fig. 6i) and gradually transitional (Fig. 6j), manifested in progressive silicification and bleaching of rocks and extinction of breccia structure.

Unlike the zone of massive siltstones and breccias of the main contact, which are epigenetic formations, the habit of the thin interbedding zone is determined by sedimentation factors.

5.3. Host rock alteration

The rocks of the Tolubai Formation and Alay limestones are pervasively hydrothermally alteration near the “main contact”. Based on the study of host rocks, three main types of gold-associated altered have

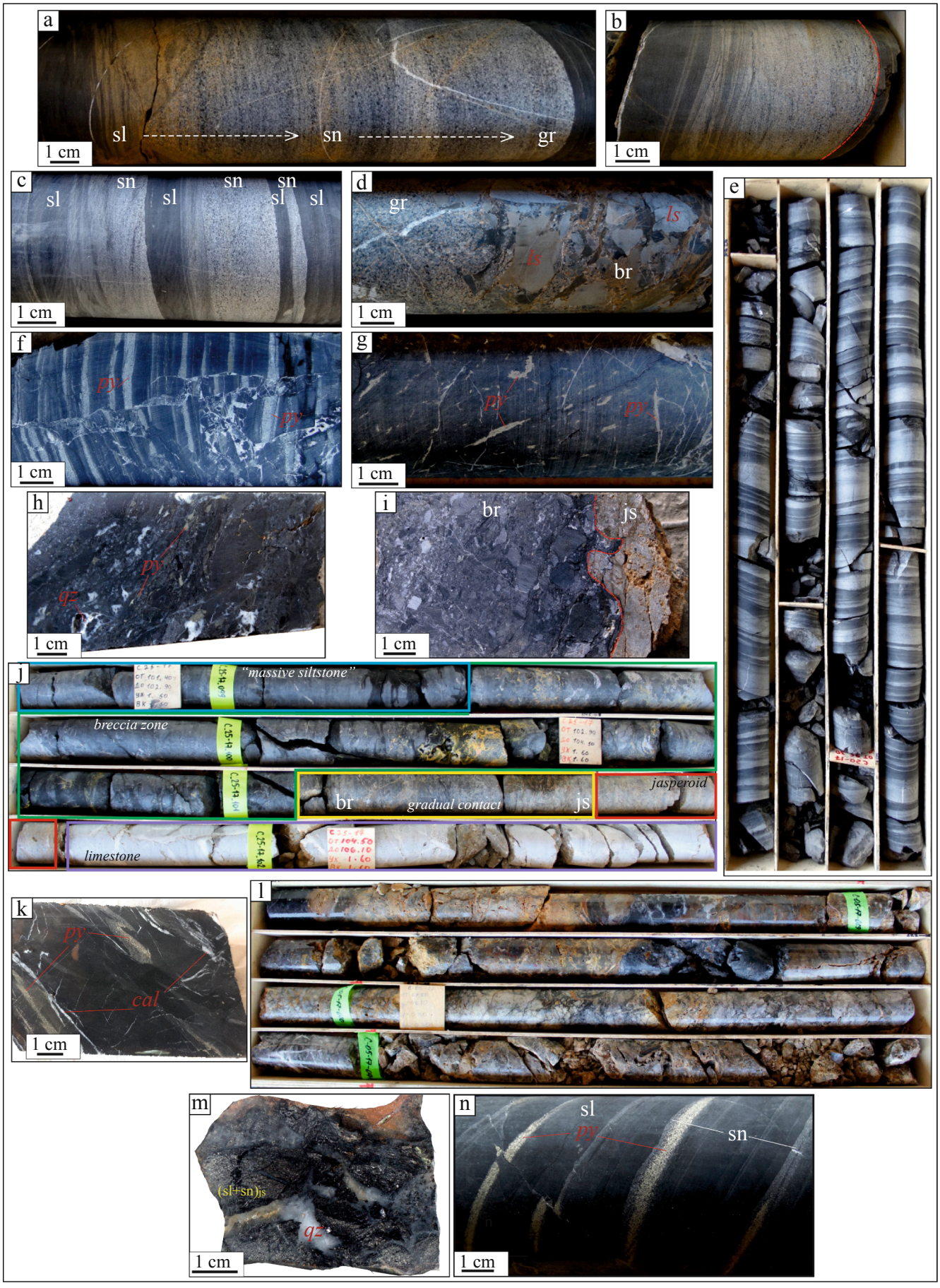

(caption on next page)

Fig. 6. Photographs showing host rocks and ore of the Chauvai (a–l, n) and Kadamzhai (m) deposits: (a) gradational sorting of detrital material; (b) base of coarse-grained layers (red line); (c) thin alternation of sandstone and siltstone layers; (d) gravel with breccia/debris-flow sediments; (e) "bundle of frequent interbedding"; (f) sandstone with disseminated sulfides; (g) "massive" siltstone with sulfide veins; (h) breccia with sulfide mineralization and quartz geodes; (i) abrupt contact between "main contact" breccia and jasperoid; (j) gradual contact between "main contact" breccia and jasperoid; (k) siltstone with disseminated sulfides and calcite veins; (l) jasperoid; (m) siliceous "main contact" breccia with quartz cement; (n) locally sulfidized siltstone and sandstone. *Note: sl – siltstone; sn – sandstone; gr – gravel; ls – limestone; br – breccia; js – jasperoid; py – pyrite; qz – quartz; cal – calcite.* (For interpretation of the references to colour in this figure legend, the reader is referred to the web version of this article.)

been recognized such as silicification, decarbonatization, and sulfidization, which are the most common types of rock alteration seen in many Carlin-type deposits (Ashley et al., 1991; Arehart, 1996; Hofstra and Cline, 2000; Cline et al., 2005; Peters et al., 2007; Pirajno, 2009; Su et al., 2009a; Xie et al., 2017).

The clastic rocks of the Tolubai Formation are stronger decarbonatized with consistent increase toward the main contact. During decarbonatization of siltstones and sandstones, a large amount of cross-cutting, rather than layer-parallel, calcite veins and veinlets formed (Fig. 6k). The source of carbonate matter for these veinlets is assumed to be the host clastic rocks.

Silicification is more distinctly manifested immediately along the main contact, where limestones are transformed into crypto- and microcrystalline rocks, which are typically vesicular and consist mainly of silica (Fig. 6l). At times, the intensity of silicification is smoothly decreasing with distance away from the contact towards the carbonate rocks series up to complete transition into unaltered limestones. The Tolubai clastic sediments are silicified to a lesser degree, however, near the main contact one can observe abundant breccia, composed of intensely silicified fragments of siltstones and sandstones cemented by chalcedonic quartz (Fig. 6m).

Results of our study indicate that economically significant gold associates with decarbonatized rocks of the Tolubai Formation. The silicified rocks are also supposed to have an elevated gold content, but its concentration does not exceed 0.1–0.5 ppm. Sb and Hg mineralization in the studied deposits is associated exclusively with jasperoids, developed mainly over limestones.

Sulfidization (iron sulfides) is developed only in the Tolubai clastic rocks. Sulfides occur as finely diffused disseminations, subconcordant microveins and zones of enrichment, cutting the veinlets (Fig. 6n). The concentration of sulfides varies from individual grains to the first percent, whereas their increased amount is not a reliable indicator of gold mineralization.

The distribution of sulfides is also controlled by the bedded structure of the formation. The most commonly enriched are thin (1–20 mm thick) interlayers of fine-grained sandstones in siltstones (Fig. 6n). These interlayers contain a rich dissemination of hydrothermal idiomorphic pyrite. In contrast, thick layers of sandstones and gritstones are depleted in sulfides or do not bear them at all. The sulfide impregnation in siltstones is so thin that it is almost invisible macroscopically.

Sulfidization processes are generally confined to the lower part of the Tolubai Formation, within about 0–20 m above the main contact. Close to the main contact, where the host rocks lose the bedded structure (zone of massive siltstones and breccias of the main contact), sulfides occur as intersecting veinlets, lenses, and vermicular segregations of 0.5–2 mm thick and 5–10 mm long, isometric clusters, as well as irregularly distributed scattered dissemination. Frequently, one can observe the replacement of scattered sulfide dissemination by orpiment.

5.4. Mineral composition

Mineral composition of the Kadamzhai and Chauvai deposits is similar to Carlin type deposits in Nevada and Guizhou province (Hofstra and Cline, 2000; Peters, 2002; Peters et al., 2007; Cline et al., 2005; Zhang et al., 2005; Su et al., 2008; Large et al., 2011). These deposits host complex ore bodies, which contain both Au and Sb-Hg. The main minerals in gold ore are pyrite, marcasite, arsenopyrite, orpiment, and realgar. Sb-Hg ores are represented by cinnabar and stibnite.

The zone of thin interbedding is dominated by impregnated and bedded ore structures (Fig. 7a). In general, siltstones are characterized by impregnated structures, while sandstone interlayers have predominantly layered textures. Individual sulfide-enriched sandstone interlayers are commonly complicated by disruptions and displacements of insignificant amplitude not exceeding the first centimeters (Fig. 7b). Cross-cutting calcite veins contain no sulfides (Fig. 7c). This ore type is typically characterized by low gold content. Sulfides are represented by pyrite and, to a lesser extent, marcasite. Arsenopyrite in these ores is rare. The size of pyrite grains and its morphological characteristics are different in sandstones and siltstones. A relatively large (up to 0.5 mm) idiomorphic pyrite dominates in sandstones (Fig. 8h). Dissemination in siltstones is represented by small idiomorphic grains of pyrite (up to 50 μm) (Fig. 8e and f), frequently framboidal pyrite (Fig. 8a). Marcasite occurs as elongated grains, in some cases its aggregates grow on pyrite of early generation (Fig. 8j).

Breccia ores are mostly manifested in the zone of massive siltstones and breccias of the main contact (Fig. 7d), while streaky ores are much less abundant (Fig. 7e). Sulfides are represented by pyrite, marcasite, and rarely arsenopyrite. A distinctive feature of this part of the section is the widespread occurrence of realgar and orpiment. In the upper part of the packet, these minerals represent rich dissemination in siltstones and sandstones, which, formed probably due to the replacing of pyrite (Fig. 7f and g). In the breccia zone of the main contact, one can observe cross-cutting veinlets of realgar and orpiment, which frequently serve as cement (Fig. 7h and 1). The widest occurrence of arsenic sulfides is confined to brecciated siltstones and sandstones, which have undergone significant decarbonatization. In some cases, the thickness of veins with realgar and orpiment reaches 1–5 cm (Fig. 7j and k). Down the sequence, where breccias are more silicified, sulfides are represented by pyrite of several generations, marcasite and arsenopyrite. Fluorite is not uncommon in silicified breccias of the main contact (Fig. 7l). Gold content in this breccia ore is up to 5 ppm.

As and Hg mineralization does not extend beyond the silicified rocks and is mostly localized in jasperoids as well as in their breccias. The major Hg and Sb minerals are represented by cinnabar and antimonite, respectively, and form veinlets and nests up to massive ores (Fig. 7m). In rare cases, quartz veinlets with antimonite and cinnabar are superimposed on the breccia of the main contact (Fig. 7n). The gangue minerals associated with Sb-Hg mineralization are represented by quartz with the subordinate calcite and fluorite. This type of ore is characterized by low gold contents, that are not higher than 0.5 ppm.

Pyrite, as major ore mineral of gold ores, occurs in the form of several generations, whose formation was successively replaced by each other. In unaltered host rocks, a significant portion of pyrite is represented by the framboids and their aggregates having isometric or oval outlines (Fig. 8a and b). We suggest that the origin of this pyrite is diagenetic. Commonly the pyrite framboids are spatially confined to the horizons enriched in organic matter (Fig. 8c). In weakly altered host rocks, the relicts of the framboidal pyrite are occasionally found in the central parts of pyrite aggregates (nodules) of irregular form, up to 100 μm in size (Fig. 8d).

The amount of sulfides in the rock typically grows with the increase in intensity of hydrothermal alteration. As the intensity of rock alteration increases, pyrite represented by small metasomatic idiomorphic grains becomes more widespread. The pyrite grain sizes in

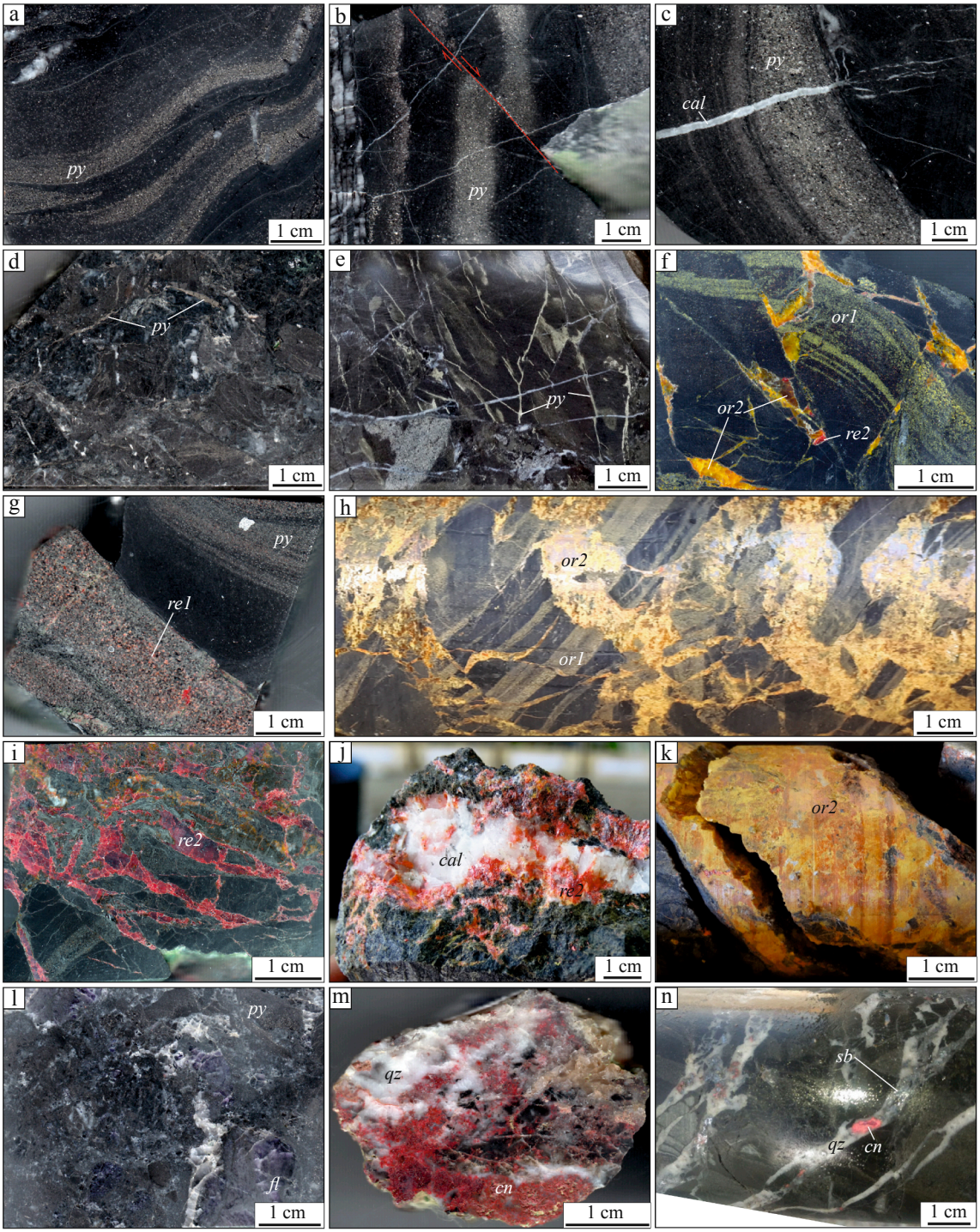

Fig. 7. Photographs showing ore structure of the Chauvai (b, e–n) and Kadamzhai (a, c, d) deposits: (a) microlayers with disseminated sulfides; (b) low amplitude displacement of sulfide microlayer; (c) calcite vein cross-cutting sulfide microlayer; (d) breccia-type ore; (e) breccia-type ore with sulfide veinlets; (f) breccia-type ore with orpiment 1 (replacing early Fe-sulfides) and veins of orpiment 2; (g) realgar 1 replacing early Fe-sulfides in sandstone layer; (h) breccia-type ore cemented by orpiment 2; (i) breccia-type ore cemented by realgar 2; (j) calcite vein with realgar 2; (k) orpiment 2 vein in breccia-type ore; (l) breccia-type ore with pyrite and fluorite; (m) quartz-cinnabar ore in apo-limestone jasperoid; (n) quartz-cinnabar-stibnite vein in breccia ore. *Note: py – pyrite; qz – quartz; cal – calcite, or1 – orpiment 1, or2 – orpiment 2, re1 – realgar 1, re2 – realgar 2, cn – cinnabar, sb – stibnite, fl – fluorite.*

siltstones are significantly lower than that in sandstones (Fig. 8e–g). Idiomorphic pyrite grains in sandstones are often zoned with abundant inclusions of nonmetallic minerals (Fig. 8h). In the zone of massive siltstones and breccias of the main contact, marcasite commonly occurs as aggregates of elongated grains ranging in size from 10 to 100 μm (Fig. 8j). In brecciated ores, clasts frequently contain various sulfide impregnations. Some fragments are characterized by the impregnation of small pyrite grains, others contain elongated marcasite grains (Fig. 8i and k). Arsenopyrite in ores is quite rare. Occasionally, single arsenopyrite grains of up to 30 μm in size intergrow with idiomorphic pyrite in sulfidized sandstones (Fig. 8l). In silicified breccias of the main contact arsenopyrite forms rims around the large clasts of idiomorphic pyrite (Fig. 8m).

The replacement of pyrite by orpiment and, to a lesser extent, by

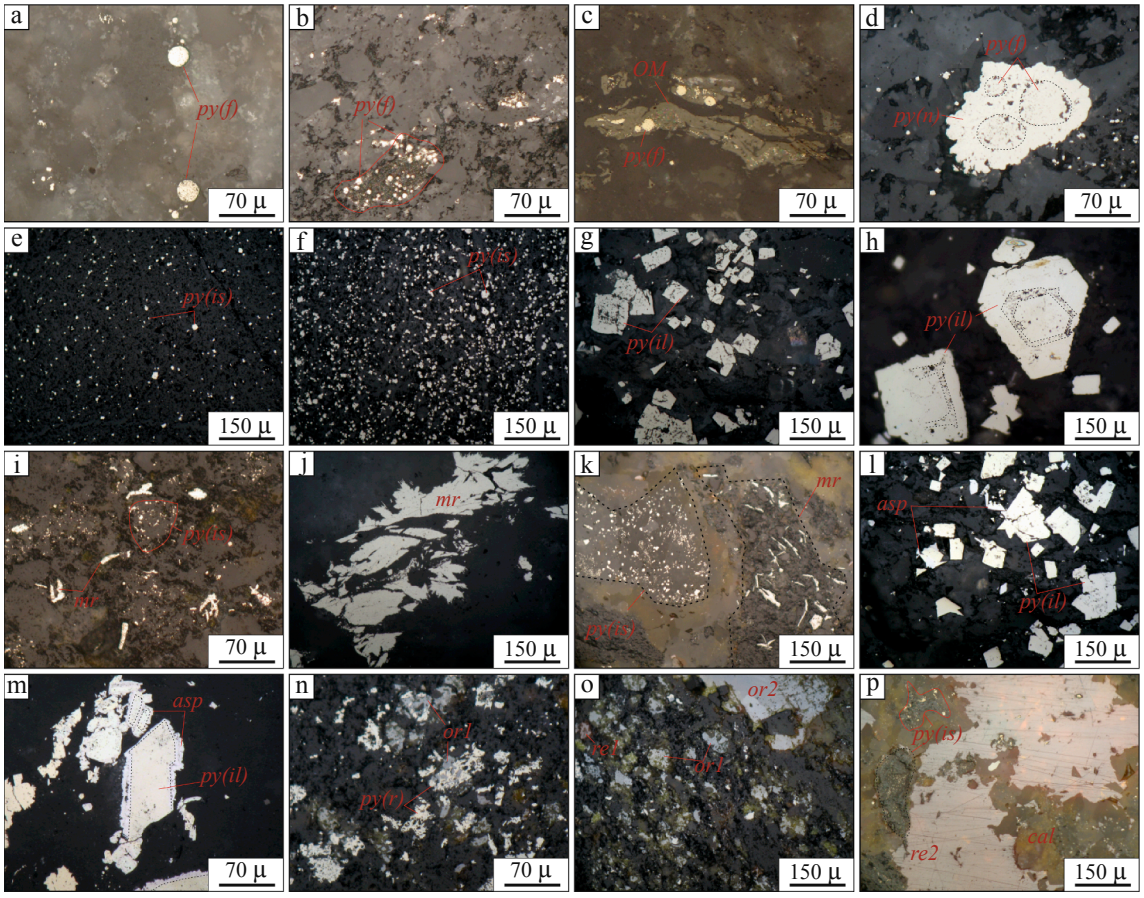

Fig. 8. Photomicrographs showing aspects of ore minerals at the Kadamzhai (i–k, m) and Chauvai (a–h, l, n–p) deposits under reflected light: (a) pyrite framboids in siltstone layer within the Tolubai Formation; (b) pyrite framboids clusters; (c) pyrite framboids in organic matter; (d) pyrite framboids included in pyrite nodules; (e) idiomorphic disseminated fine-grained pyrite in siltstone (low sulfide content ore); (f) idiomorphic disseminated fine-grained pyrite in siltstone (high sulfide content ore); (g) idiomorphic disseminated coarse-grained pyrite in sandstone; (h) zonal grains of idiomorphic coarse-grained pyrite in sandstone; (i) breccia type ore with mineralized clasts and elongate grains of marcasite; (j) elongate grains of marcasite in breccia type ore; (k) idiomorphic disseminated fine-grained pyrite and elongate grains of marcasite within and clasts in brecciated rocks; (l) idiomorphic disseminated coarse-grained pyrite and arsenopyrite in sandstone; (m) idiomorphic coarse-grained pyrite with rims of arsenopyrite in breccia type ore; (n) relict of pyrite replaced by orpiment; (o) disseminated fine-grained realgar and orpiment in sandstone and calcite-orpiment vein; (p) calcite-realgar vein, which contains fragments of siltstone with disseminated fine-grained pyrite. *Note: py(f) – pyrite framboid; py(n) – nodules of pyrite; py(is) – idiomorphic fine-grained pyrite; py(il) – idiomorphic coarse-grained pyrite; py(r) – relict of pyrite; mr – marcasite; asp – arsenopyrite; or1 – disseminated fine-grained orpiment 1, or2 – coarse-grained orpiment in vein;, re1 – disseminated fine-grained realgar 1, re2 – coarse-grained realgar in vein; cal – calcite; OM – organic matter.*

realgar is widespread in breccias of the main contact (Fig. 8n) Thus, orpiment forms complete pseudomorphs after pyrite aggregates. Fragments of mineralized siltstones and sandstones are cut by calcite veinlets with realgar and orpiment (Fig. 8o). In thicker veins there are fragments of sulfidized siltstones (Fig. 8p).

In general, it may be inferred that ore minerals are represented by pyrite of several generations (framboidal–nodular–idiomorphic), marcasite, arsenopyrite, realgar and orpiment. No native gold was found in the ores. The antimony-mercury mineralization, composed mainly of antimonite and cinnabar, is intersecting the gold mineralization.

5.5. Ore geochemistry

Selected results of ICP-MS analysis of host rocks and ores are shown in Table 1.

Unaltered sedimentary rocks of the Tolubai Formation consist of alternating layers of siltstones, sandstones, and gravel. No gold and silver were found in assays of the unaltered rocks. The contents of Hg and Tl are below detection limits. The Sb content is at a very low level ranging from 0.2 to 2 ppm. The As content varied from 6 to 57, with an average value of 24 ppm. The contents of Ba and Sr are relatively high due to the high content of carbonate material in unaltered rocks.

In the zone of thin-bedded siltstones, especially where disseminated and layered sulfidization is manifested, the gold content ranges between 0.42 and 0.71 ppm. High gold contents strongly correlate with: As (9072 and 3253 ppm), Hg (51 and 38 ppm), Sb (98.6 and 79.1 ppm), and Tl (26.5 and 17.9 ppm), respectively. The concentrations of these elements in the gold-free samples correspond to those in unaltered rocks. The mineralized siltstone varieties of this zone reveal lower Ba and Sr contents, which, most likely, can be due to decarbonatization processes. Similar geochemical features were also observed in for the zone of massive siltstones. Although the assays did not reveal economically significant gold contents (0.34–0.51 ppm Au), these modified rocks are characterized by a relatively high content of As, Hg, Sb, and Tl. In addition, there is a significant decrease (by an order of magnitude) in the concentration of Ba and Sr.

The gold content in gold-bearing ore, represented by mineralized altered breccias of the main contact, varies from 0.42 to 4.16 ppm. Silver is practically absent in ores, with its maximum concentrations being 2.2 ppm. The arsenic content is abnormally high ranging from 4346 to more than 50,000 ppm (the upper limit of determination). The concentrations of other Carlin-suite elements are as follows: Hg from 37 to 232 ppm (mean value 110 ppm), Sb – from 51.6 to 1926.3 ppm (mean value 446.5 ppm), and Tl – from 5.9 to 18 ppm (mean value

Table 1
Geochemical data of representative and variably mineralized rocks of the Chauvai deposit.

Rock type	#	Au	Ag	As	Ba	Bi	Co	Cr	Cu	Hg	Mo	Nb	Ni	Pb	Rb	Sb	Se	Sn	Sr	Ta	Te	Tl	U	V	W	Zn
Unaltered host rock (siltstone. Sandstone and gravel of the Tolubay Fm)	1	0.00	0.0	57	338	0.15	9.7	6.6	38	0	1.4	0.10	27	12.8	9.92	2.0	1	0.0	455	0.00	0	0.0	1.25	20	0	66
	2	0.00	0.0	6	212	0.18	8.6	7.3	50	0	0.4	0.07	19	8.5	7.03	0.3	1	0.3	203	0.00	0	0.0	0.46	9	0	42
	3	0.00	0.0	11	260	0.15	6.4	5.6	71	0	1.0	0.06	17	7.0	5.38	0.4	1	0.3	327	0.00	0	0.0	0.19	8	0	40
	4	0.00	0.0	25	109	0.10	2.3	2.5	101	0	0.2	0.07	6	8.1	3.13	0.2	1	0.0	502	0.00	0	0.0	0.16	5	0	21
	5	0.00	0.0	21	320	0.22	3.2	7.0	42	0	0.4	0.06	8	7.8	6.51	0.3	1	0.5	235	0.00	0	0.0	0.18	6	0	26
Rythmic siltstone (Locally sulfidized siltstone and sandstone)	1	0.00	1.0	132	387	0.17	11.6	8.3	49	1	0.9	0.10	33	13.8	11.25	1.8	2	0.2	335	0.00	5	0.1	0.74	24	1	75
	2	0.00	1.0	696	123	0.14	12.5	5.8	43	1	1.2	0.10	34	14.7	7.79	3.3	2	0.2	401	0.00	5	0.1	0.39	17	1	56
	3	0.42	0.0	9072	111	0.22	13.8	8.0	54	51	1.1	0.08	34	17.4	11.44	98.6	2	0.0	111	0.00	0	26.5	0.49	18	1	89
	4	0.71	0.0	3253	126	0.22	13.2	7.5	54	38	1.7	0.08	35	17.3	11.42	79.1	1	0.0	126	0.00	0	17.9	0.52	14	1	89
	5	0.00	0.0	724	318	0.18	11.9	6.4	40	0	1.1	0.08	28	14.7	9.23	2.3	2	0.4	383	0.00	0	0.1	0.67	16	0	66
Massive siltstone	1	0.34	1.2	810	44	0.26	16.9	9.0	67	22	1.5	0.07	44	20.6	11.13	38.3	1	0.0	34	0.00	0	9.2	0.63	14	4	98
	2	0.51	0.0	1021	50	0.28	16.3	7.6	63	18	2.1	0.07	43	19.8	12.57	46.9	2	0.0	59	0.00	0	6.1	0.56	15	2	106
Main contact Breccia	1	1.46	1.0	20,245	100	0.22	15.1	6.7	65	124	1.4	0.06	40	18.8	9.27	438.0	3	0.3	26	0.00	5	15.8	0.68	9	1	90
	2	1.27	1.0	50,000	53	0.24	13.7	7.7	65	232	1.3	0.07	36	17.4	9.33	1926.3	6	0.3	21	0.00	5	14.9	0.59	10	4	89
	3	0.55	1.0	11,200	79	0.39	14.9	7.6	66	172	1.5	0.07	39	20.0	10.06	166.6	2	0.2	34	0.00	5	8.6	0.61	10	2	97
	4	1.30	1.0	31,432	62	0.26	17.5	7.2	63	113	1.3	0.10	46	18.9	11.71	574.8	4	0.4	40	0.00	5	12.6	0.67	12	2	98
	5	2.35	1.0	41,329	37	0.25	15.5	10.4	75	100	0.9	0.08	41	20.8	11.27	987.9	4	0.4	27	0.00	5	18.0	0.67	12	1	96
	6	2.21	0.0	32,868	92	0.24	12.7	8.2	55	62	1.7	0.08	34	16.5	10.89	111.2	2	0.5	180	0.00	0	10.0	0.70	15	2	87
	7	3.44	1.2	50,000	54	0.19	10.3	8.5	67	46	1.2	0.10	29	14.7	7.85	160.1	4	0.4	294	0.00	8	16.4	0.77	15	4	71
	8	4.16	2.2	31,533	100	0.20	11.1	11.9	150	73	2.9	0.10	27	16.7	8.78	150.7	2	0.5	271	0.00	0	13.0	1.26	21	5	89
	9	1.22	1.0	4346	108	0.27	14.2	10.5	66	81	1.9	0.07	38	18.7	10.48	51.6	1	0.5	165	0.00	0	14.3	0.77	18	3	75
	10	0.42	0.0	14,426	108	0.29	14.6	17.7	71	37	2.5	0.05	40	18.4	12.47	110.7	1	0.4	38	0.00	0	5.9	0.95	18	1	103
	11	1.57	0.0	27,421	91	0.31	18.0	10.3	127	167	2.5	0.06	45	21.5	10.79	233.5	1	0.6	74	0.00	0	11.0	0.89	15	1	101
Jasperoid Breccia (Siliceous main contact breccia)	1	0.56	0.0	2803	164	0.28	15.8	9.6	63	36	1.4	0.07	40	18.0	12.41	20.4	1	0.5	122	0.00	0	4.9	0.65	20	2	63
	2	0.27	0.0	576	169	0.42	24.4	10.3	99	68	0.6	0.06	69	22.4	14.50	37.8	1	0.6	69	0.00	0	3.2	0.41	16	2	46
	3	0.83	0.0	497	169	0.43	21.6	8.1	81	62	1.2	0.06	63	27.4	10.83	22.3	1	0.5	34	0.00	0	4.4	0.50	10	1	70
	4	0.21	1.0	182	78	0.27	17.6	19.7	89	44	1.0	0.06	47	18.5	12.36	282.6	2	0.3	41	0.00	5	3.6	0.56	17	2	52
	5	0.22	1.0	159	134	0.35	17.4	16.9	88	104	2.5	0.08	46	25.1	11.58	40.2	2	0.3	43	0.00	5	4.7	1.50	14	2	64
Jasperoid (Siliceous limestone of the Alay Succession)	1	0.35	1.6	213	277	0.42	14.4	46.1	82	83	1.5	0.26	47	49.8	61.71	981.0	2	0.9	217	0.04	5	7.2	3.89	59	2	55
	2	0.34	1.2	421	327	0.32	18.8	41.9	86	48	1.4	0.22	55	24.1	58.74	2440.9	2	0.8	239	0.03	5	10.7	3.71	54	2	154
	3	0.43	1.7	200	397	0.30	10.8	41.6	369	515	1.8	0.17	34	170.2	46.59	911.7	3	0.6	270	0.02	5	3.5	6.99	48	1	100
	4	0.27	2.3	324	129	0.24	11.4	15.3	87	1000	5.7	0.05	49	15.8	8.05	1364.8	4	1.0	53	0.00	0	20.0	1.71	9	4	177
	5	0.31	3.2	384	172	0.20	17.4	13.0	92	993	2.0	0.04	59	14.5	6.83	614.6	2	0.6	49	0.00	0	13.4	1.27	9	4	204

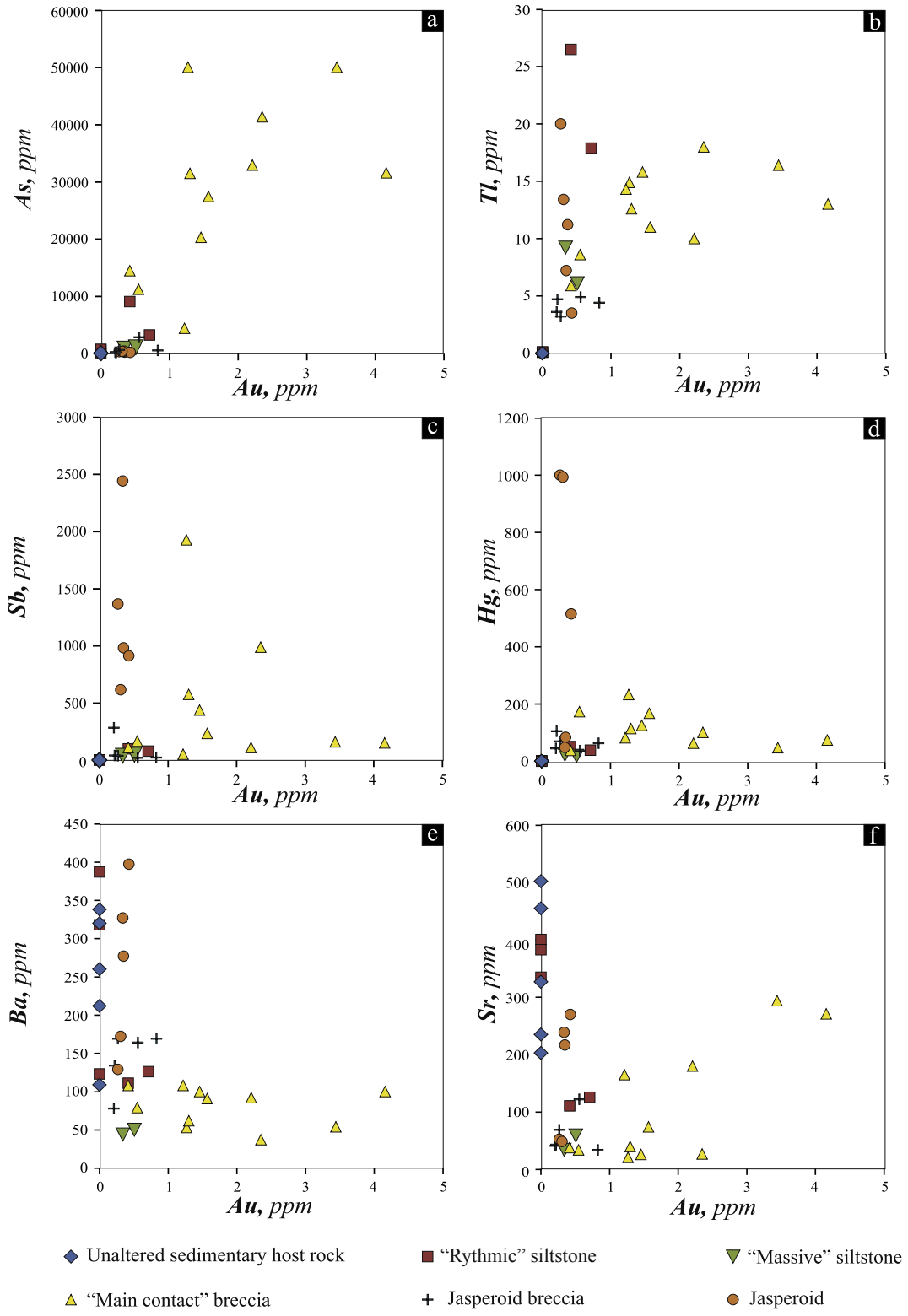

Fig. 9. Bivariate plots for arsenic, thallium, antimony, mercury, barium and strontium against gold for rocks and ores of the Chauvai deposit. (a) arsenic–gold; (b) thallium–gold; (c) antimony–gold; (d) mercury–gold; (e) barium–gold; (f) strontium–gold.

12.8 ppm). The content of base metals (Pb, Zn, and Cu) is similar to that from the unaltered or weakly altered rocks. Of the rock-forming elements, Ba and Sr contents are significantly lower (relative to unaltered rocks). This decrease is supposedly related to the decarbonatization and silicification of rocks, which are associated with the formation of mineralization.

In the zone of intense silicification of breccias at the main contact (the zone of jasperoid breccias) the gold content is not high, ranging from 0.21 to 0.83 ppm. The contents of As, Hg, Sb, and Tl consistently decrease. The strontium content is significantly lower than in unaltered rocks, but barium concentration is slightly higher than in non-silicified breccias. This may be due to the formation of a rare impregnation of

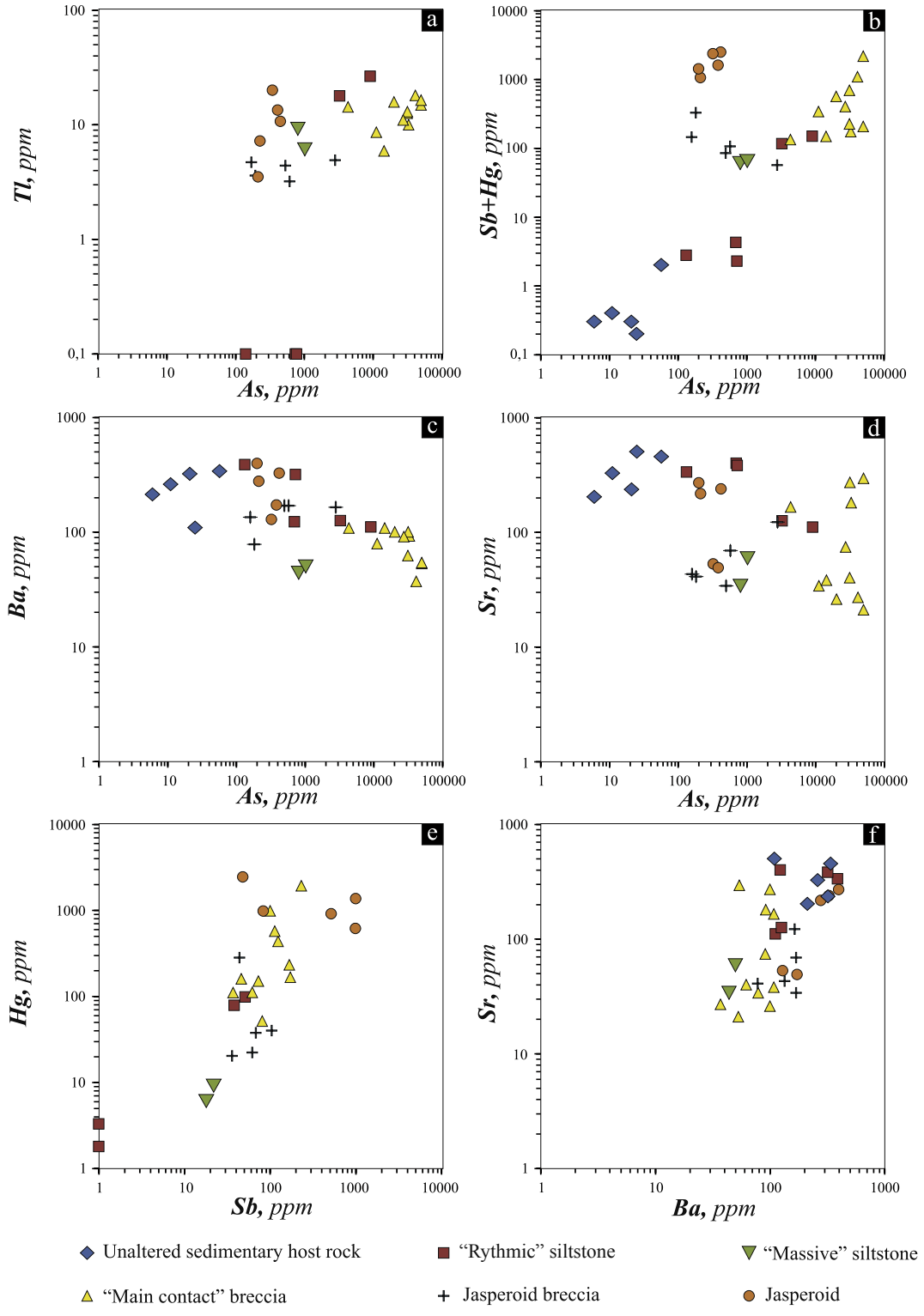

Fig. 10. Bivariate plots of selected minor elements for rocks and ores of the Chauvai deposit. (a) thallium–arsenic; (b) antimony and mercury–arsenic; (c) barium–arsenic; (d) strontium–arsenic; (e) mercury–antimony; (c) strontium–barium.

barite together with fluorite.

Jasperoids have low gold contents of 0.34 ppm on average. Silver grade reaches as high as 3.2 ppm. A relatively high silver content probably may be due to high concentrations of antimony. Jasperoids have high Hg and Sb contents, up to 1000 and 2440.9 ppm, respectively. Such elevated contents of these elements are consistent with petrographic evidence and field observations, according to which Sb-Hg mineralization is confined specifically to jasperoids developed over limestones. The Sr content shows a challenging regularity. Two groups of jasperoids are distinguished: the first group hosts 250 ppm Sr on average, while the second group is significantly depleted in strontium, with an average value of 50 ppm. This fact can be explained by incomplete silicification of limestones of the first group. The barium content is quite high (up to 397 ppm). Considering intensive metasomatic alteration of limestones as well as depletion in strontium, such high barium values can be associated with barite mineralization

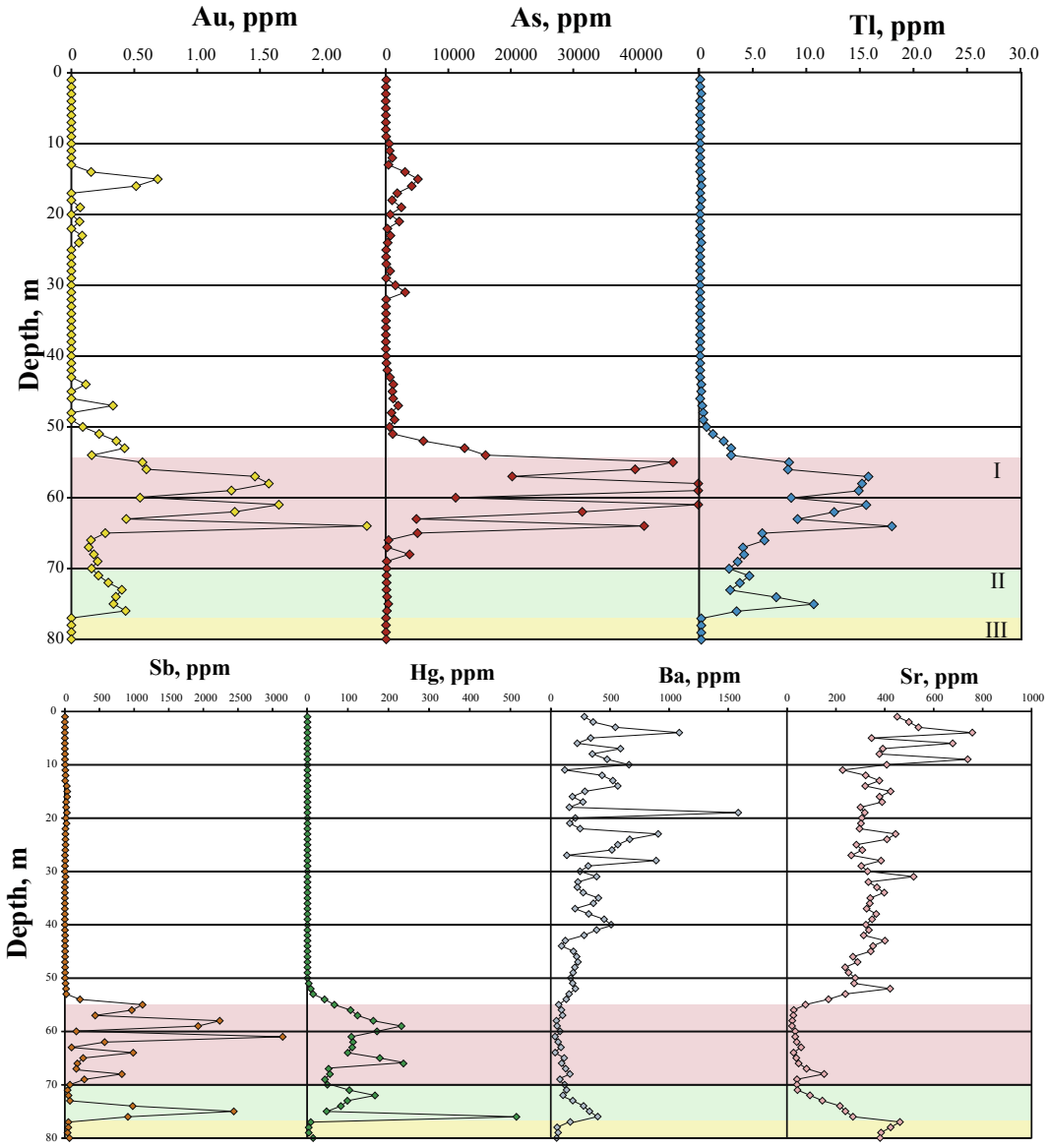

Fig. 11. Gold and trace elements in core sample at the Chauvai deposit. Plots illustrate strong positive correlation between Au, As, and Tl, strong reverse correlation for Ba and Sr against Au, and weak positive correlation for Hg and Sb against Au with separated anomaly these elements in jasperoid. *Note: I – zone of "ritmic" siltstone and "main contact" breccia (55–70 m); II – zone of jasperoid breccia and jasperoid (70–76 m); III – unaltered limestone (76–80 m).*

accompanying Hg-Sb mineralization at the deposit. On the other hand, it cannot be ruled out that elevated barium contents are associated with relicts of metasomatically unaltered limestones.

6. Discussion

6.1. Geochemical signature

Sedimentary rock-hosted gold deposits, including Carlin-type gold deposits, are characterized by a specific suite of trace elements. In a broad sense, this set consists of Au, As, Sb, Hg, and Tl (Zhang and Zhang, 2003; Zhang et al., 2005; Peters et al., 2007; Large et al., 2011). Orogenic sedimentary rock-hosted gold deposits usually contain significant concentrations of Au, As, and Sb (Goldfarb et al., 2005; Large et al., 2011; Goldfarb and Groves, 2015; Nevolko et al., 2017; Yudovskaya et al., 2016), whereas, a suite of trace elements, Au, (As, Sb, Hg, and Tl) is inherent only to Carlin-type deposits (Hofstra and Cline, 2000; Cline et al., 2005; Peters et al., 2007). However, Au, As, Sb, Hg, and Tl rarely form composite economic ore deposits. There are examples where Carlin-suite elements are present in insignificant amount and appears only as "geochemical signature" of mineralization. Some deposits are complex and contain significant resources of mercury, antimony, arsenic and less often thallium. For example, the giant Wuchuan and Wanshan mercury deposits (> 10,000 t of Hg) in Guizhou province have low gold concentrations and moderate antimony and arsenic concentrations. Similarly, the giant Dachang antimony deposit (> 500,000 t Sb) in Guizhou province has low concentrations of Au, As, Sb, and Hg (Hu et al., 2002). Instead, one of the elements is usually dominant and the others are subordinate. So, the amounts of As, Sb, and Hg in the ores at the Banqi, Getang, Zimudang, and Lannigou deposits in southwest Guizhou province are of no commercial importance and could never be mined independently (Peters, 2002; Yan et al., 2018).

Newly obtained geochemistry data of the Chauvai deposit (Fig. 9a and b), convincingly demonstrate a strong positive correlation of gold with arsenic and less pronounced correlation of gold with thallium. Since geochemical data from the deposits show positive correlations between gold and arsenic and no native gold have been observed, we

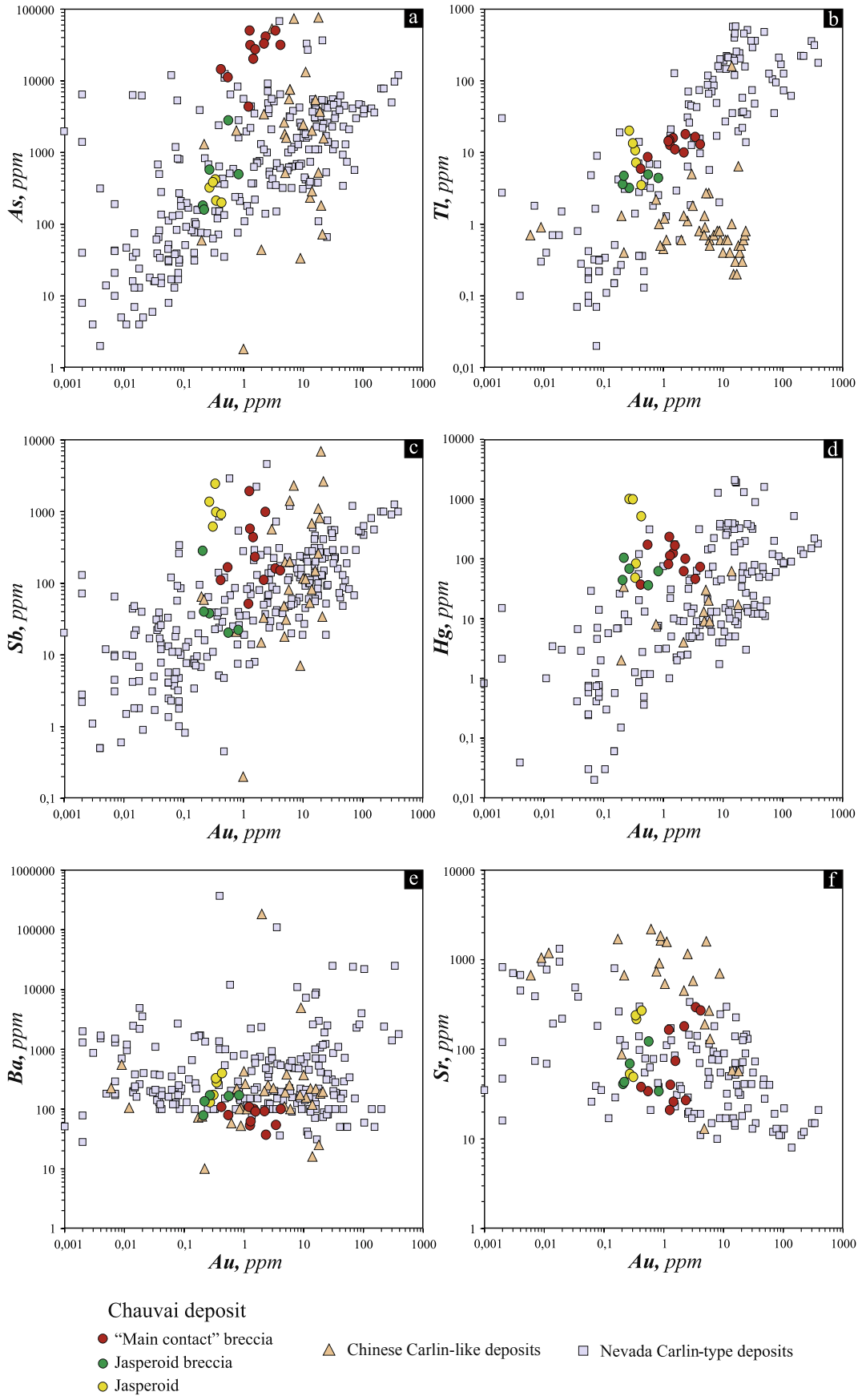

(caption on next page)

Fig. 12. Bivariate plots for arsenic, thallium, antimony, mercury, barium and strontium against gold for ores of the Chauvai deposit, China, and Nevada Carlin type gold deposits. (a) arsenic–gold; (b) thallium–gold; (c) antimony–gold; (d) mercury–gold; (e) barium–gold; (f) strontium–gold. Data from Chinese deposits: Danzhai (Lu, 1994), Yata, Getang, and Shuiyindong (Sanchahe) (Ashley et al., 1991), Bojitian (Hu et al., 2017a,b). Data for Nevada deposits: Beast (Ressel et al., 2000a,b), Griffin and Meikle (Ressel et al., 2000b), Getchell (Cail and Cline, 2001), Betze-Post, Golden April, Meikle, Ren, and Rodeo (Emsbo et al., 2003), Betze-Post (Kesler et al., 2003), and Pipeline (Hickey et al., 2014).

suggest that there are occurrence of invisible gold in arsenous-pyrite (or marcasite) and arsenopyrite.

Bivariate plots for antimony and mercury against gold (Fig. 9c and d) do not show strong correlations between gold and any of these elements. In addition, for all types of ores and hydrothermally altered host rocks there is a strong positive correlation in pairs of Tl vs. As and Sb vs. Hg (Fig. 10a and e). The total content of antimony and mercury also shows a direct correlation with the arsenic concentration (Fig. 10b). This fact can be explained that this mineralization was formed as a result of a single process and Carlin-suite elements were added to the rocks by the same hydrothermal fluid.

Concentrations of copper, lead, zinc, and tin do not consistently correlate with gold values. Barium generally correlates well with strontium (Fig. 10f). The bivariate plot for barium and strontium shows strong positive correlation, but bivariate plots for barium and strontium against gold and arsenic revealed a reverse correlation (Figs. 9e, f and 10c, d, f). Thus, as the degree of hydrothermal alteration of host rocks increases (with an increase of gold and arsenic contents), the concentration level of barium and strontium decreases. This can be explained by the fact that in unaltered host rocks, barium and strontium are concentrated in the carbonate material. Since the deposit formation associated with decarbonatization and silicification alteration types, these elements have been removed from mineralization zone.

Relationship and correlation between Carlin-suite elements at the Chauvai deposit are shown in Fig. 11, which illustrated content of Au, As, Tl, Sb, Hg, Ba, and Sr downhole as plotted line graph. Unaltered host siltstone and sandstone contain significant amount of barium and strontium, however concentration of these elements almost completely decreases at a depth of 55 m. From here and to a depth of 70 m, clastic rocks have been intensely altered (decarbonatization and sulfidization type) and contain high level of arsenic, thallium and gold. Antimony and mercury mineralization is also confined to this zone of altered rocks, but apart from been located within a zone of jasperoid breccia and jasperoid (silicification alteration type).

Following Hou et al. (2016) and Tan et al. (2015), we suppose that deposition and spatial distribution of Carlin-suite elements depends on structural-lithological factors, rather than on a paragenetic sequence, as is shown in Ashley et al. (1991) and Hu et al. (2002). Different host rocks are also preferentially mineralized by different elements. The gold ores (Au-As-Tl) are mainly hosted in siltstones and their breccia, whereas the mercury and antimony mineralization occur chiefly in altered carbonate rocks (jasperoid). The same is observed in other Carlin-type deposits. According to Hu et al. (2001), Su et al. (2012), and Tan et al. (2015) mercury mineralization associated with the Shuiyindong (Sanchahe) gold deposit in southwest Guizhou occurs mainly within a carbonate horizon of the Changxing Formation, but gold mineralization is restricted to the lower mudstone units of this formation.

Based on our new data on textural features and mineral composition of ore, we suggest that the weak positive correlation for antimony and mercury against arsenic is more likely a consequence of different structural control of mineralization, rather than the paragenetic sequence.

The similar distribution patterns of Carlin-suite elements are known in many Carlin-type gold deposits located in different region. With the aim of comparison geochemistry signature of the Kyrgyz deposits with typical Carlin-type deposits we used available data from nine Nevada and five China deposits (Ashley et al., 1991; Lu, 1994; Ressel et al., 2000a,b; Cail and Cline, 2001; Emsbo et al., 2003; Kesler et al., 2003; Cline et al., 2013; Hickey et al., 2014; Tan et al., 2015; Hu et al., 2017a,b).

As one can see on Figs. 12 and 13, in general, the fields of concentration level for Catlin-suite elements completely overlap. In addition, there are correlations between pairs of elements described above. The geochemical features of the Chauvai deposit are similar to the Chinese and Nevada deposits, although there are some particular aspects. For example, the Kyrgyz Carlin-type deposits are characterized by a higher concentration of arsenic (Fig. 12). The concentration of thallium is slightly higher than in Chinese deposits, but it corresponds to the average content of Nevada ones. Taking into account the data in Table 1 and Figs. 12 and 13, we conclude that geochemical signature of the Chauvai deposit is more similar to the deposits in China, but they are characterized by an higher concentration of thallium.

6.2. Tectonic setting

Gold mineralization at the Kadamzhai and Chauvai deposits is accompanied by antimony and mercury ores. Available K-Ar data for sericite from jasperoid, according to Nikiforov (1969), Fedorchuk (1985), and Yao et al. (2015), clearly show Permian to Triassic ages for Kadamzhai Sb (280–240 Ma) and Haydarkan deposits (230–236 Ma and 244–268 Ma). Furthermore, published geochronological reports for regional antimony-polymetallic mineralization and orogenic gold deposits of the South Tien Shan constrain their formation to the Early Permian–Middle Triassic (Yakubchuk et al., 2002; Mao et al., 2004; Yang et al., 2006; Morelli et al., 2007; Chen et al., 2012; Yao et al., 2015;), a time broadly coeval with the post-collision processes (McCann et al., 2013; Konopelko et al., 2018).

So, tectonic settings for gold mineralization at the Kadamjai and Chauvai deposits, proposed by us, are transpressional regime and similar to that forming the Carlin-like gold deposits in the Yunnan–Guizhou–Guangxi and western Qinling regions (Mao et al., 2002; Peters, 2002; Zhang and Zhang, 2003; Su et al., 2009b; Chen et al., 2015; Hu et al., 2017a,b; Pi et al., 2017). However, Kyrgyz Carlin-type gold deposits have been formed in a quite different setting from those in Nevada, where formation correlates in time with back-arc extension (Hofstra and Cline, 2000; Cline et al., 2005).

We propose that the Kadamzhai and Chauvai gold deposits are inferred to have formed after peak deformation during the final stages of transpession and extension of the South Tien Shan collisional orogeny. Genesis and spatial distribution of structurally-controlled deposits located in collisional orogen is best interpreted by crustal continuum model (Groves et al., 1998; Chen, 2013; Goldfarb et al., 2014) and is also applicable for studied deposits. The metamorphic fluid and basinal fluids, which were probably derived from epizonal to metamorphic devolatilisation of host strata, were channeled along regional faults and unconformities, and the metals were leached from the country rocks and deposited in structural traps.

7. Conclusion

Major geological and geochemical features of the Kadamzhai and Chauvai deposits include:

1. mineralization along the main contact of the Tolubai Formation and Alay limestone;
2. low-temperature hydrothermal Sb-Hg mineral systems;
3. silicification, decarbonatization, and sulfidization;
4. metallic mineral assemblage (pyrite + marcasite + arsenopyrite +

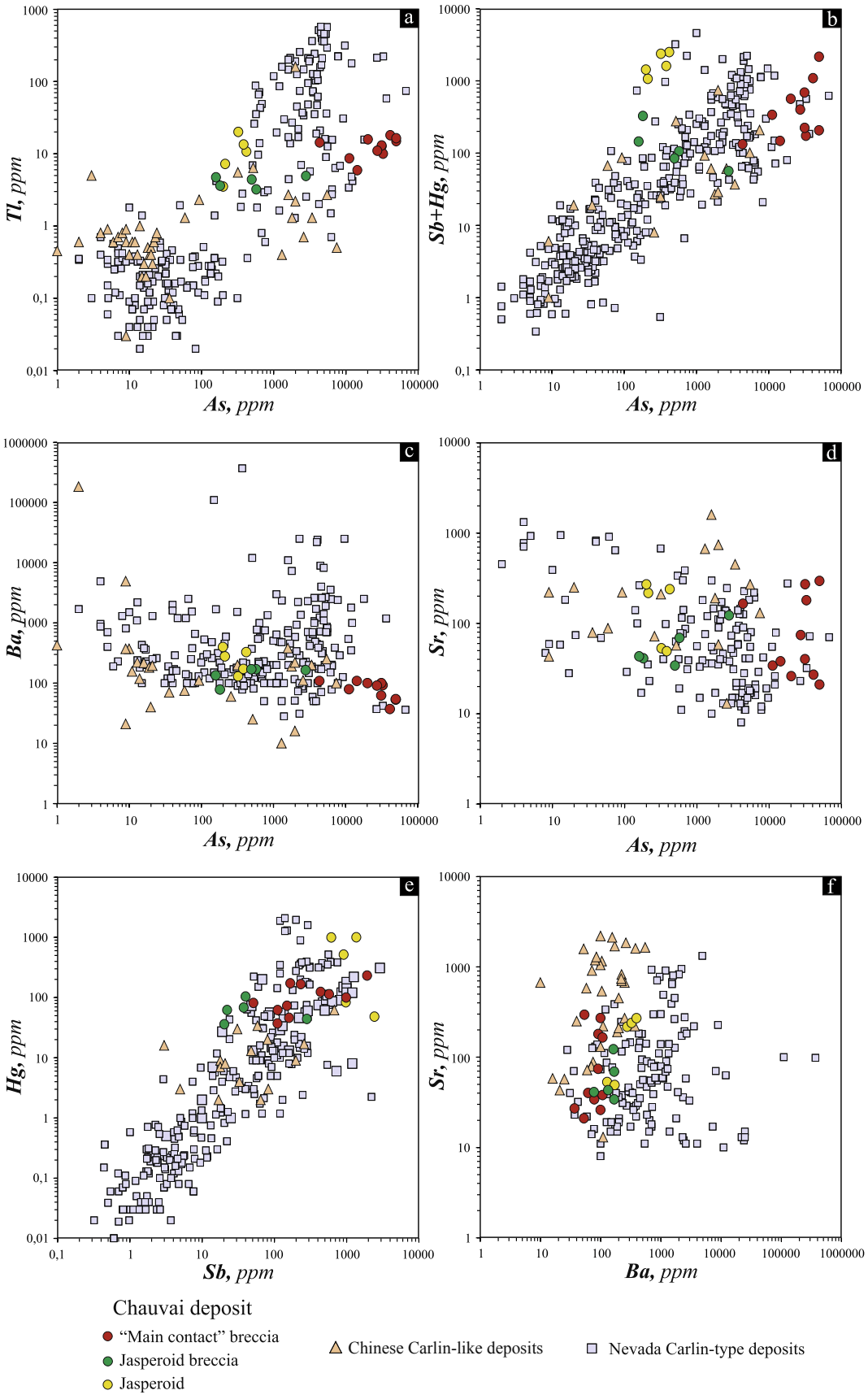

Fig. 13. Bivariate plots of selected minor elements for rocks and ores of the Chauvai deposit, Chinese, and Nevada Carlin-type gold deposits (a) thallium–arsenic; (b) antimony and mercury–arsenic; (c) barium–arsenic; (d) strontium–arsenic; (e) mercury–antimony; (c) strontium–barium. Data from Chinese deposits: Danzhai (Lu, 1994), Yata, Getang, and Shuiyindong (Sanchahe) (Ashley et al., 1991), Bojitian (Hu et al., 2017a,b). Data for Nevada deposits: Beast (Ressel et al., 2000a,b), Griffin and Meikle (Ressel et al., 2000b), Getchell (Cail and Cline, 2001), Betze-Post, Golden April, Meikle, Ren, and Rodeo (Emsbo et al., 2003), Betze-Post (Kesler et al., 2003), and Pipeline (Hickey et al., 2014).

realgar + opriment), typical of Carlin-type gold deposits;
5. invisible gold (no observed native gold), associated with arsenic, antimony, mercury, and thallium (Carlin-suite elements), with high gold-silver ratios;
6. structural control and dissemination to the wall rocks, which is similar to the Chinese and United States Carlin deposits;
7. alignment of Kadamzhai and Chauvai deposits, together with Severnyi Aktash, Obdilla and Shambesai Carlin-type deposits, along the 40-km-long trends;
8. transpressional structural control, similar to Carlin-type gold deposits in the Yunnan–Guizhou–Guangxi and western Qinling regions.

If we use the list of Carlin characteristics from Hofstra et al. (1999), Hofstra and Cline (2000), Cline et al. (2005), and Peters et al. (2007), Kadamzhai and Chauvai deposits fit quite well. So, based on new ore geology, geochemical signatures and mineral composition of the Kadamzhai and Chauvai deposits, we suggest that the Kadamzhai and Chauvai deposits are Carlin-type gold deposits in the South-Fergana Sb-Hg metallogenic belt.

Acknowledgments

This study was conducted under state assignment projects of IGM SB RAS (№ 0330-2016-0001). We thank Realgold Resources Corp. for their support and access to mineral deposits in Kyrgyzstan. We are thank to Dr. Boris Trifonov and an anonymous reviewer for their comments and suggestion. We are extremely grateful for the critical comments of the Associate Editor Dr. Alexander Yakubchuk, which have all greatly enhanced the quality of the manuscript.

References

Alekseev, D.V., Degtyarev, E.V., Kotov, A.B., Sal'nikova, E.B., Tret'yakov, A.A., Yakovleva, S.Z., Anisimova, I.V., Shatagin, K.N., 2009. Late Paleozoic subductional and collisional igneous complexes in the Naryn segment of the Middle Tien Shan (Kyrgyzstan). Dokl. Earth Sci. 42, 760–763.
Arehart, G.B., 1996. Characteristics and origin of sediment-hosted disseminated gold deposits: a review. Ore Geol. Rev. 11, 383–403.
Ashley, R.P., Cunningham, C.G., Bostick, N.H., Dean, W.E., Chou, I.M., 1991. Geology and geochemistry of three sedimentary rock-hosted disseminated gold deposits in Guizhou province, People's Republic of China. Ore Geol. Rev. 6, 133–151.
Biske, Yu.S., 1996. Paleozoic Structure and History of Southern Tien-Shan. Leningrad University, Leningrad, pp. 187 (in Russian).
Biske, Yu.S., Seltmann, R., 2010. Paleozoic Tian-Shan as a transitional region between the Rheic and Urals-Turkestan oceans. Gondwana Res. 17, 602–613.
Burtman, V.S., 2006. Tien Shan and High Asia. Tectonics and Geodynamics in the Paleozoic. GEOS, Moscow, pp. 214 (in Russian).
Cail, T.L., Cline, J.S., 2001. Alteration associated with gold deposition at the Getchell Carlin-type gold deposit, north-central Nevada. Econ. Geol. 96, 1343–1359.
Chen, H.Y., Chen, Y.J., Baker, M.J., 2012. Evolution of ore-forming fluids in the Sawayaerdun gold deposit in the southwestern Chinese Tianshan metallogenic belt, Northwest China. J. Asian Earth Sci. 49, 131–144.
Chen, M., Mao, J., Chao, L., Zhang, Z., Dang, Y., 2015. Re–Os isochron ages for arsenopyrite from Carlin-like gold deposits in the Yunnan–Guizhou–Guangxi "golden triangle", southwestern China. Ore Geol. Rev. 64, 316–327.
Chen, Y.J., 2013. The development of continental collision metallogeny and its application. Acta Petrol. Sin. 29, 1–17 (in Chinese with English abstract).
Cline, J.S., Hofstra, A.H., Muntean, J.L., Tosdal, R.M., Hickey, K.A., 2005. Carlin-type gold deposits in Nevada: critical geological characteristics and viable models. Econ. Geol. 100th Anniversary Volume, 451–484.
Cline, J.S., Muntean, J.L., Gu, X.X., Xia, Y., 2013. A comparison of Carlin-type gold deposits: Guizhou Province, golden triangle, southwest China, and northern Nevada, USA. Earth Sci. Front. 20 (1), 1–18.
Dodonova, T.A., Pomazkov, K.D., Pomazkov, Ya.K., 1984. Endogenic Geological Formations of Kyrgyzia. Magmatic Formations vol. 1. "Yilim" Publishing House, Frunze, Kyrgyz SSR, pp. 212 (in Russian).
Emsbo, P., Hofstra, A.H., Lauha, E.A., Griffin, G.L., Hutchinson, R.W., 2003. Origin of high-grade gold ore, source of ore fluid components, and genesis of the Meikle and neighboring Carlin-type deposits, northern Carlin trend, Nevada. Econ. Geol. 98 (6), 1069–1105.
Fedorchuk, V.P., 1985. Geology of Antimony. Nedra, Moscow, pp. 267 (in Russian).
Ghes, M.D., 2008. Terrain Structure and Geodynamic Evolution of Caledonian Tian-Shan. National Academy of Science of Kyrgyzstan, Bishkek, pp. 159 (In Russian).
Goldfarb, R.J., Baker, T., Dube, B., Groves, D.I., Hart, C.J.R., Gosselin, R., 2005. Distribution, character, and genesis of gold deposits in metamorphic terranes. In: Hedenquist, J.W. (Ed.), Economic Geology 100th Anniversary Volume: Littleton, Colorado, Econ. Geol. pp. 407–450.
Goldfarb, R.J., Taylor, R.D., Collins, G.S., Goryachev, N.A., Orlandini, O.F., 2014. Phanerozoic continental growth and gold metallogeny of Asia. Gondwana Res. 25, 48–102.
Goldfarb, R.J., Groves, D.I., 2015. Orogenic gold: common or evolving fluid and metal sources through time. Lithos 233, 2–26.
Groves, D.I., Goldfarb, R.J., Gebre-Mariam, M., Hagemann, S.G., Robert, F., 1998. Orogenic gold deposits: a proposed classification in the context of their crustal distribution and relationship to other gold deposit types. Ore Geol. Rev. 13, 7–27.
Hickey, K.A., Ahmed, A.D., Barker, S.L., Leonardson, R., 2014. Fault-controlled lateral fluid flow underneath and into a Carlin-type gold deposit: isotopic and geochemical footprints. Econ. Geol. 109 (5), 1431–1460.
Hofstra, A.H., Snee, L.W., Rye, R.O., Folger, H.W., Phinisey, J.D., Loranger, R.J., Dahl, A.R., Naeser, C.W., Stein, H.J., Lewchuk, M., 1999. Age constraints on Jerritt Canyon and other Carlin-type gold deposits in the western United States – relation to mid-Tertiary extension and magmatism. Econ. Geol. 94, 769–802.
Hofstra, A.H., Cline, J.S., 2000. Characteristics and models for Carlin-type gold deposits. In: In: Hagemann, S.G., Brown, P.E. (Eds.), Rev. in Econ. Geol., vol. 13. pp. 163–214.
Hou, L., Peng, H., Ding, J., Zhang, J., Zhu, S., Wu, S., Wu, Y., Ouyang, H., 2016. Textures and in situ chemical and isotopic analyses of pyrite, Huijiabao trend, Youjiang Basin, China: implications for paragenesis and source of sulfur. Econ. Geol. 111, 331–353.
Hu, K., Pan, M., Cao, J., Liu, Y., Han, S., 2017a. The Au-hosting minerals and process of formation of the Carlin-type Bojitian deposit, Southwestern China. Geofluids Article ID 2417209.
Hu, R.-Z., Su, W.-C., Bi, X.-W., Tu, G.-Z., Hofstra, A.H., 2002. Geology and geochemistry of Carlin-type gold deposits in China. Miner. Deposita 37, 378–392.
Hu, R., Fu, S., Huang, Y., Zhou, M.-F., Fu, S., Zhao, C., Wang, Y., Bi, X., Xiao, J., 2017b. The giant South China Mesozoic low-temperature metallogenic domain: reviews and a new geodynamic model. J. Asian Earth Sci. 137, 9–34.
Jahn, B.M., Wu, F.Y., Chen, B., 2000. Granitoids of the Central Asian Orogenic Belt and continental growth in the Phanerozoic. Earth Environ. Sci. Trans. R. Soc. 91, 181–193.
Kesler, S.E., Fortuna, J., Ye, Z., Alt, J.C., Core, D.P., Zohar, P., Borhauer, J., Chryssoulis, S.L., 2003. Evaluation of the role of sulfidation in deposition of gold, screamer section of the Betze-Post Carlin-type deposit, Nevada. Econ. Geol. 98, 1137–1157.
Kirwin, D.J., Becker, A., Banduruk, I., Lueck, B., 2017. The Carlin-type Hg, Sb, As, Au, F, Tl deposits of the southwest Kyrgyz Republic. Soc. Econ. Geol. Newslett. 110 (1), 14–18.
Konopelko, D., Wilde, S.A., Seltmann, R., Romer, R.L., Biske, Yu.S., 2018. Early Permian intrusions of the Alai range: Understanding tectonic settings of Hercynian post-collisional magmatism in the South Tien Shan, Kyrgyzstan. Lithos 302–303, 405–420.
Large, R.R., Bull, S.W., Maslennikov, V.V., 2011. A carbonaceous sedimentary source-rock model for carlin-type and orogenic gold deposits. Econ. Geol. 106 (3), 331–358.
Li, H.H., Qiu, R.Z., Tan, Y.J., Qi, S.J., Wang, Q.M., Wang, K.A., Han, J.X., 2010. The Exploration and Development Guidelines of Mineral Resources in the Five Countries in Central Asian. China University of Geosciences Press, Wuhai, pp. 207 (in Chinese).
Lu, G.Q., 1994. A Genetic Link Between the Gold-mercury Mineralization and Petroleum Evolution – A Case of the Danzhai Gold-mercury Deposit (PhD thesis). Universite du Quebec, Chicoutimi, Quebec.
Mao, J.W., Qiu, Y.M., Goldfarb, R.J., Zhang, Z.C., Garwin, S., Ren, F.S., 2002. Geology, distribution, and classification of gold deposits in the western Qinling belt, central China. Miner. Deposita 37 (3–4), 352–377.
Mao, J., Konopelko, D., Seltmann, R., Lehmann, B., Chen, Wen, Wang, Yitian, Eklund, O., Usubaliev, T., 2004. Postcollisional age of the Kumtor gold deposit and timing of Hercynian events in the Tien Shan, Kyrgyzstan. Econ. Geol. 99, 1771–1780.
McCann, T., Nurtaev, B., Kharin, V., Valdivia-Manchego, M., 2013. Ordovician-Carboniferous tectono-sedimentary evolution of the North Nuratau region, Uzbekistan (Westernmost Tien Shan). Tectonophysics 590, 196–213.
Morelli, R.M., Creaser, R.A., Seltmann, R., Stuart, F.M., Selby, D., Graupner, T., 2007. Age and source constraints for the giant Muruntau gold deposit, Uzbekistan, from coupled Re-Os-He isotopes in arsenopyrite. Geology 35 (9), 795–798.
Nenakhov, V.M., Belov, S.I., 1996. Main features of intrusive magmatism of Turkestan-Alay. Vestnik Voronezhskogo Universiteta, Seriya Geologiya 1, 84–89 (in Russian).
Nenakhov, V.M., Ivanikov, V.V., Kuznetsov, L.V., Strik, Y.N., 1992. Methods of Investigation and Geological Mapping of Collisional Granitoids. "Roskomnedra" Publishing House, Moscow, pp. 101 (in Russian).
Nenakhov, V.M., Vaulin, O.V., 1992. Paleogeodynamic settings and evolution of ore formation in Turkestan-Alay. Sov. Geol. 8, 43–48 (in Russian).
Nevolko, P.A., Tran, T.H., Redin, Y.O., Tran, T.A., Ngo, T.P., Vu, H.L., Dultsev, V.F., Pham, T.D., Ngo, T.H., 2017. Geology, mineralogy, geochemistry and d34S of sedimentary rock-hosted Au deposits in Song Hien structure, NE Vietnam. Ore Geol. Rev. 84, 273–288.
Nikiforov, N.A., 1969. Mercury and Antimony Mineralization of South Tien Shan. Ilim, Frunze, pp. 246 (in Russian).
Osmonbetov, K.O., Knauf, V.I. (Eds.), 1982. Stratified and Intrusive Formations of Kyrgyzia. "Yilim" Publishing House, Frunze, Kyrgyz SSR (in Russian).
Peters, S.G., 2002. Geology, Geochemistry, and Geophysics of Sedimentary-Hosted Au Deposits in P.R. China. U.S. Geological Survey Open-File Report, 02–131, Version 1.0. http://geopubs.wr.usgs.gov/open-file/of02-131/.
Peters, S.G., Huang, J.Z., Li, Z.P., Jing, C.G., 2007. Sedimentary rock-hosted Au deposits of the Dian–Qian–Gui area, Guizhou, and Yunnan Provinces, and Guangxi District, China. Ore Geol. Rev. 31, 170–204.
Pi, Q.H., Hu, R.Z., Xiong, B., Li, Q., Zhong, R., 2017. In situ SIMS U-Pb dating of hydrothermal rutile: reliable age for the Zhesang Carlin-type gold deposit in the golden

triangle region, SW China. Miner. Deposita 52, 1179–1190.
Pirajno, F., 2009. Hydrothermal Processes and Mineral System. Springer, Berlin, pp. 1250.
Porter, T.M., 2006. The Tien Shan belt: golden heart of Central Asia. The Gangue 88 (1), 4–5.
Ressel, M.W., Noble, D.C., Heizler, M.T., Volk, J.A., Lamb, J.B., Park, D.E., Conrad, J.E., Mortensen, J.K., 2000a. Gold-mineralized Eocene dikes at Griffin and Meikle: bearing on the age and origin of deposits of the Carlin trend, Nevada. In: Geology and Ore Deposits 2000: The Great Basin and Beyond Proceedings Volume I, pp. 79–101.
Ressel, M.W., Noble, D.C., Henry, C.D., Trudel, W.S., 2000b. Dike-hosted ores of the Beast deposit and the importance of Eocene magmatism in gold mineralization of the Carlin Trend, Nevada. Econ. Geol. 95, 1417–1444.
Rickleman, D.E., Archangelski, A., Jackson, M., Lysenko, V., Story, J., Zholdoshov, T., Atabaev, O., 2011. Carlin-type Au potential of the Turkestan-Alai and South Fergana segments, Southern Tianshan, Kyrgyzstan. Association of Applied Geochemists. International Applied Geochemical Symposium, 25th, Rovaniemi, Finland, August 22–29, 2011, Poster.
Seltmann, R., Graupner, T., Klemd, R., Kempe, U., Shatov, V., 2003. Criteria for an exploration model for Muruntau style deposits. CERCAMS Report (Unpublished). NHM, London, pp. 92.
Seltmann, R., Shatov, V., Yakubchuk, A.S., Lehmann, B., Jingwen, M., Fedorenko, O., Isakhodjaev, B., Nikonorov, V., Minaev, 2004. Mineral deposit types of central Asia; new exploration models based on modern geodynamic background (IGCP-473 progress report). International Geological Congress, 32nd, Florence, Italy, August 20–28, 2004. International Union of Geological Sciences 215-1:993.
Sengör, A.M.C., Natalin, B.A., Burtman, V.S., 1993. Evolution of the Altaid tectonic collage and Paleozoic crustal growth in Eurasia. Nature 364, 299–307.
Sengör, A.M.C., Natalin, B.A., 1996. Paleotectonics of Asia: fragments and synthesis. In: Yin, A., Harrison, M. (Eds.), The Tectonic Evolution of Asia. Cambridge University Press, pp. 486–640.
Solomovich, L.I., 2007. Postcollisional magmatism in the South Tien Shan Variscan Orogenic Belt, Kyrgyzstan: evidence for high-temperature and high-pressure collision. J. Asian Earth Sci. 30, 142–153.
Su, W., Xia, B., Zhang, H., Zhang, X., Hu, R., 2008. Visible gold in arsenian pyrite at the Shuiyindong Carlin-type gold deposit, Guizhou, China: implications for the environment and processes of ore formation. Ore Geol. Rev. 33, 667–679.
Su, W.C., Heinrich, C.A., Pettke, T., Zhang, X.C., Hu, R.Z., Xia, B., 2009a. Sediment hosted gold deposits in Guizhou, China: products of wall-rock sulfidation by deep crustal fluids. Econ. Geol. 104, 73–93.
Su, W.C., Hu, R.Z., Xia, B., Xia, Y., Liu, Y., 2009b. Calcite Sm-Nd isochron age of the Shuiyindong Carlin-type gold deposit, Guizhou, China. Chem. Geol. 258, 269–274.
Su, W.C., Zhang, H.T., Hu, R.Z., Ge, X., Xia, B., Chen, Y.Y., Zhu, C., 2012. Mineralogy and geochemistry of gold-bearing arsenian pyrite from the Shuiyindong Carlin-type gold deposit, Guizhou, China: implications for gold depositional processes. Miner. Deposita 47, 653–662.
Tan, Q.P., Xia, Y., Xie, Z.J., Yan, J., 2015. Migration paths and precipitation mechanisms of ore-forming fluids at the Shuiyindong Carlin-type gold deposit, Guizhou, China. Ore Geol. Rev. 69, 140–156.
Vaulyn, O.V., 2016. Structurally-Material Complexes of Turkestan-Alay. Geodynamics. Geochemistry. Metallogeny. Ore Content. Rokizol, Bishkek, pp. 281 (in Russian).
Windley, B.F., Alexeiev, D.V., Xiao, W., Kröner, A., Badarch, G., 2007. Tectonic models for accretion of the Central Asian Orogenic belt. J. Geol. Soc. Lond. 164, 31–47.
Xie, Z.J., Xia, Y., Cline, J.S., Yan, B.W., Wang, Z.P., Tan, Q.P., Wei, D.T., 2017. Comparison of the native antimony-bearing painting gold deposit, Guizhou Province, China, with Carlin-type gold deposits, Nevada, USA. Miner. Deposita 52 (1), 69–84.
Yakubchuk, A., 2004. Architecture and mineral deposit settings of the Altaid orogenic collage: a revised model. J. Asian Earth Sci. 23, 761–779.
Yakubchuk, A., Cole, A., Seltmann, R., Shatov, V., 2002. Tectonic setting, characteristics, and regional exploration criteria for gold mineralization in the Altaid orogenic collage: the Tien Shan province as a key example. Soc. Econ. Geol. Spec. Publ. 9, 177–201.
Yan, J., Hu, R., Liu, S., Lin, Y., Zhang, J., Fu, S., 2018. NanoSIMS element mapping and sulfur isotope analysis of Au-bearing pyrite from Lannigou Carlin-type Au deposit in SW China: new insights into the origin and evolution of Au-bearing fluids. Ore Geol. Rev. 92, 29–41.
Yang, F.Q., Mao, J.W., Wang, Y.T., Bierlein, F.P., 2006. Geology and geochemistry of the Bulong quartz-barite vein-type gold deposit in the Xinjiang Uygur autonomous region, China. Ore Geol. Rev. 29, 52–76.
Yao, W.G., Lv, P.R., Wu, L., Hong, J., Yang, B., Jia, Q.Z., Li, B.Q., 2015. Geological characteristics of dominant mineral resources of the Tianshan Mountains in Kyrgyzstan and their prospecting potential. Geol. Bull. China 34, 710–725 (in Chinese with English abstract).
Yudovskaya, M.A., Distler, V.V., Prokofiev, V.Yu., Akinfiev, N.N., 2016. Gold mineralisation and orogenic metamorphism in the Lena province of Siberia as assessed from Chertovo Koryto and Sukhoi Log deposits. Geosci. Front. 7, 453–481.
Zhang, F., Zhang, J., 2003. Geological–geochemical characteristics of Carlin-and Carlin-like-type gold deposits in South Qinling mountains. Chin. J. Geochem. 22, 11–22.
Zhang, X.C., Hofstra, A.H., Hu, R.-Z., Emsbo, P., Su, W., Ridley, W.I., 2005. Geochemistry and δ34S of ores and ore stage iron sulfides in Carlin-type gold deposits, Dian- Qian-Gui area, China: Implications for ore genesis. In: Mao, J.W., Bierlein, F.P. (Eds.), Mineral Deposits Research: Meeting the Global Challenge, 2. Springer-Verlag, Heidelberg, pp. 1107–1110.
Zhou, Z., Chen, Z., Han, F., Han, S., Wang, Z., Xiao, W., Shen, T., Wu, J., 2017. Fluid inclusion and isotope geochemistry of the Atebayue Sb deposit, South Tian Shan Orogen, Kyrgyzstan. Geol. J. 1–11.
Zubtsov, Ye.I., Porshniakov, G.S., Yagovkin, A.V., 1974. New Sketch of pre-Mesozoic Tectonics of Tian-Shan. Dokl. Acad. Nauk SSSR 217 (5), 1153–1156 (In Russian).